Consideration of Initial Cloud Droplet Size Distribution Shapes in Quantifying Different Entrainment-Mixing Mechanisms

Shi Luo[1], Chunsong Lu[1*], Yangang Liu[2*], Wenhua Gao[3], Lei Zhu[1], Xiaoqi Xu[1], Junjun Li[1], Xiaohao Guo[4]

1. Collaborative Innovation Center on Forecast and Evaluation of Meteorological Disasters (CIC-FEMD)/ Key Laboratory for Aerosol-Cloud-Precipitation of China Meteorological Administration, Nanjing University of Information Science & Technology, Nanjing, China
2. Environmental and Climate Sciences Department, Brookhaven National Laboratory, Upton, New York, US
3. State Key Laboratory of Severe Weather, Chinese Academy of Meteorological Sciences, Beijing, China
4. Suzhou Meteorological Bureau, Suzhou, China

Corresponding author: Chunsong Lu; Yangang Liu

luchunsong110@gmail.com; lyg@bnl.gov

This article has been accepted for publication and undergone full peer review but has not been through the copyediting, typesetting, pagination and proofreading process, which may lead to differences between this version and the Version of Record. Please cite this article as doi: 10.1029/2020JD034455.

Abstract

Entrainment-mixing process significantly affects cloud micro/macrophysics and the evaluation of aerosol indirect effects. However, it is still an open question as to how to quantify entrainment-mixing mechanism for broad cloud droplet size distributions (CDSDs). Here, CDSDs with different spectral widths are used to initialize the Explicit Mixing Parcel Model to address this problem, and microphysical properties are compared for different CDSD widths. For relatively broad CDSDs, as the number concentration and liquid water content decrease, the volume-mean radius and mean radius increase, which is opposite to the scenario for relatively narrow CDSDs and the homogeneous/inhomogeneous conceptual model. For the relatively broad CDSDs, such relationships could be mistaken as inhomogeneous mixing with subsequent ascent in analysis of the conventional microphysical mixing diagram. This then causes traditional homogenous mixing degrees to be unrealistically negative and not applicable for relatively broad CDSDs. New measures are introduced to explicitly account for the effect of CDSD spectral shapes on quantifying entrainment-mixing mechanism. The new measures yield reasonable ranges of values that conform to the dynamical measures such as the Damköhler and transitional scale numbers, and their temporal variation can be explained physically. This study extends the measures of homogeneous mixing degrees from narrow to broad CDSDs, and sheds new light on the consideration of CDSD shapes in parameterizations of entrainment-mixing mechanism.

Key points:

- Microphysical properties and entrainment-mixing mechanism are dissected for different cloud droplet spectral widths.
- Inhomogeneous mixing with subsequent ascent could be mistakenly identified and traditional homogeneous mixing degrees are not applicable for broad spectra.
- New measures of homogeneous mixing degrees are introduced and verified.

1. Introduction

Clouds are critical to weather and climate, hydrological cycle, and radiative balance (*Wood*, 2012; *P Yang et al.*, 2015; *Del Genio et al.*, 2015; *Guo et al.*, 2019; *Randall et al.*, 2019a; *Li et al.*, 2020; *F Zhang et al.*, 2018a, 2018b; *Lin et al.*, 2020), and as such, the accurate descriptions of macro and microphysical cloud processes/properties are essential to improving weather and climate simulations/forecasts/projections (*M Zhang et al.*, 2013; *Y Wang et al.*, 2013; *Donner et al.*, 2016; *W Gao et al.*, 2016; *G Zhang et al.*, 2019; *Liu*, 2019; *Randall et al.*, 2019b; *Xu et al.*, 2020). One important process is the small-scale entrainment-mixing process between subsaturated droplet-free air and cloud volume containing droplets (*Baker et al.*, 1980; *Beals et al.*, 2015; *Kumar et al.*, 2018). This process is considered as one of the promising candidates that contribute to the increase in the width of cloud droplet size distribution (CDSD) and the formation of liquid-phase precipitation (*Beard and Ochs*, 1993; *Yum*, 1998; *Small and Chuang*, 2008; *Cooper et al.*, 2013; *F Yang et al.*, 2016; *Lu et al.*, 2018a; *Hoffmann and Feingold*, 2019). Additionally, entrainment-mixing has significant impacts on aerosol-cloud interactions, cloud-climate feedbacks, amongst other processes (*Ackerman et al.*, 2004; *Xue and Feingold*, 2006; *Grabowski*, 2006; *Kim et al.*, 2008; *Del Genio and Wu*, 2010; *Xu and Xue*, 2015). Understanding the detailed entrainment-mixing mechanism and their impacts is still challenging (*Liu et al.*, 2002; *Morrison and Grabowski*, 2008; *Hill et al.*, 2009; *Jarecka et al.*, 2013; *Tölle and Krueger*, 2014; *Yum et al.*, 2015; *C Zhao et al.*, 2019), although this process has been intensely studied over the past several decades.

Based on the evolution of microphysical processes during mixing and evaporation, the homogeneous and inhomogeneous mixing conceptual model is often used to analyze entrainment-mixing mechanism (e.g., *Baker et al*., 1980; *Beals et al*., 2015; *Gerber et al*., 2008; *Lehmann et al*., 2009). In a uniform, unsaturated environment, when homogeneous entrainment-mixing occurs, droplets evaporate at the same time and as a result, droplet size and number concentration (n_c) decrease. When the entrainment-mixing mechanism is extreme inhomogeneous, some droplets do not evaporate and others experience complete evaporation. Therefore, droplet size is the same as that in adiabatic clouds with decreasing n_c. Qualitatively, the entrainment-mixing mechanism in the cloud is reported to be homogeneous (*Jensen et al.*, 1985; *Yum and Hudson*, 2001; *Burnet and Brenguier*, 2007; *Lu et al.*, 2013c; *Yeom et al.*, 2017) or extreme inhomogeneous (*Pawlowska and Brenguier*, 2000; *Burnet and Brenguier*, 2007; *Haman et al.*, 2007; *Freud et al.*, 2011).

Besides qualitative analyses, quantitative descriptions of entrainment-mixing are also performed in some studies. For example, *Morrison and Grabowski* (2008) defined a property to distinguish different entrainment-mixing mechanisms quantitatively. The mechanism can also be quantified by slopes in the relationship between droplet radius and liquid water content (LWC) or n_c (*J Wang et al.*, 2009; *Andrejczuk et al.*, 2009). *Gerber et al.* (2008) defined the inhomogeneous fraction based on a diagram of the relationship between effective radius and LWC. *Lu et al*. (2013b, 2014b) proposed four measures of homogeneous mixing degree to quantify mixing types based on the similar diagrams as mentioned above. These methods are further applied to identify the entrainment-mixing types and establish parameterizations of entrainment-mixing mechanism (*Lu et al.*, 2014a, 2018b; *Z Gao et al.*, 2018; *Luo et al.*, 2020; *S Gao et al.*, 2020).

However, the conventional mixing diagrams and the associated quantifications are essentially determined by droplet volume-mean radius (r_v), n_c, and LWC; initial CDSDs are often explicitly or implicitly assumed to be narrow or even monodisperse (*Kumar et al.*, 2012, 2014; *Lu et al.*, 2013b; *Tölle and Krueger*, 2014; *Z Gao et al.*, 2018). As argued in *Liu et al.* (1995), *Chandrakar et al.* (2020), and *Wu and McFarquhar* (2018), the shape of CDSD is critical for understanding cloud processes. In fact, the CDSDs in adiabatic clouds are not necessarily narrow as they can be broadened due to processes such as turbulent fluctuation and/or giant cloud condensation nuclei (*Johnson*, 1982; *Feingold et al.*, 1999; *Yin et al.*, 2000; *McGraw and Liu*, 2006; *Chandrakar et al.*, 2016; *Desai et al.*, 2018; *Lu et al.*, 2018a; *Prabhakaran et al.*, 2020). The measurements from cloud-penetrating airplane observations indicate that the CDSDs are usually broad (*Small and Chuang*, 2008; *Gerber et al.*, 2008; *Lu et al.*, 2018a; *Yum et al.*, 2015).

Luo et al. (2020) qualitatively found that the initial CDSD width is an important factor affecting droplet evaporation and CDSD shape during mixing and evaporation. This study extends *Luo et al.* (2020) to address the following questions: 1) Are the traditional homogeneous mixing degrees still applicable to describe entrainment-mixing mechanism for broad initial CDSDs? 2) If not, how to quantify the effect of the CDSD shape on entrainment-mixing process? To answer these questions, we run the Explicit Mixing Parcel Model (EMPM) (*Kerstein*, 1988, 1992; *Krueger et al.*, 1997; *Tölle and Krueger*, 2014; *Su et al.*, 1998) using different initial CDSD shapes. Effects of CDSD shapes on the evolution of microphysical properties and traditional homogeneous mixing degrees are analyzed. A new method for measuring the homogeneity of the mixing process is introduced and shown to be applicable to both narrow and broad initial CDSDs.

The rest of the paper is structured as follows. Section 2 shows the microphysical measures of entrainment-mixing process, the initial CDSDs, and the EMPM model. Section 3 presents the characteristics of microphysics for different CDSD shapes during mixing, the new measures of entrainment-mixing process applicable to different CDSD shapes, and physical supports for using the new measures. The conclusions and discussions are given in section 4.

2. Methods and Model

2.1 Microphysical Measures of Entrainment-Mixing

From the microphysical perspective, our previous studies have measured the entrainment-mixing process through four homogeneous mixing degrees (ψ_j, where j is from 1 to 4) (*Lu et al.*, 2013b, 2014a, 2014b; *Z Gao et al.*, 2018; *Luo et al.*, 2020; *S Gao et al.*, 2020):

$$\psi_1 = \frac{2}{\pi}\tan^{-1}\left(\frac{\frac{r_v^{\,3}}{r_{va}^{\,3}} - 1}{\frac{n_c}{n_a} - \frac{n_h}{n_a}}\right), \tag{1a}$$

$$n_h = \chi n_a . \tag{1b}$$

$$\psi_2 = \frac{1}{2}\left(\frac{n_c - n_i}{n_h - n_i} + \frac{r_v^{\,3} - r_{va}^{\,3}}{r_{vh}^{\,3} - r_{va}^{\,3}}\right), \tag{2a}$$

$$r_{vh}^3 = \frac{n_c}{n_h} r_v^3 \ , \tag{2b}$$

$$n_i = \frac{r_v^3}{r_{va}^3} n_c \ . \tag{2c}$$

$$\psi_3 = \frac{\ln n_c - \ln n_i}{\ln n_h - \ln n_i} = \frac{\ln r_v{}^3 - \ln r_{va}{}^3}{\ln r_{vh}{}^3 - \ln r_{va}{}^3} \tag{3}$$

$$\psi_4 = \frac{1 - (\frac{r_v}{r_{va}})^3}{1 - \frac{1}{\chi}\frac{LWC}{LWC_a}} \tag{4}$$

where n_a, r_{va} and LWC_a represent the droplet number concentration, volume-mean radius and liquid water content in adiabatic clouds, respectively; n_h and n_i are the droplet number concentrations after homogeneous mixing and extreme inhomogeneous mixing, respectively; r_{vh} is the volume-mean radius after homogeneous mixing; χ is the adiabatic cloud fraction during mixing between cloud and droplet-free air. When the mixing process is extreme inhomogeneous, ψ equals 0; in contrast, when ψ equals 1, the process is homogeneous.

2.2 Initial CDSDs

Without loss of generality, the initial CDSDs before entrainment-mixing are assumed to follow a Gamma size distribution, which is widely used in the literature (*Liu et al.*, 2002; *McFarquhar et al.*, 2015; *Lu et al.*, 2020)

$$n(r) = N_0 r^{\mu} e^{-\lambda r} \tag{5}$$

where r is the droplet radius; the droplet number concentration in the radius range [r, $r+dr$] is $n(r)dr$; N_0, λ and μ are the intercept, slope and shape parameters, respectively;

μ is a function of relative dispersion (d: standard deviation (σ) divided by mean radius (r_m)). A larger μ indicates a narrower CDSD. Different CDSDs ranging from 1 – 25 μm in radius are produced by altering μ. The CDSDs are set to have the same initial liquid water content of 0.5 g m^{-3} and initial droplet number concentration (n_d) of 119.4 cm^{-3}, which gives r_v of 10.0 μm. The values of μ are set to be 0.5, 2.0, 10.0, and 40.0, which correspond to d of 0.70, 0.55, 0.3, and 0.16, respectively. The monodisperse CDSD is also included. Therefore, the initial CDSDs are classified into three groups: monodisperse, narrow polydisperse (μ = 10.0, 40.0), and broad polydisperse (μ = 0.5, 2.0). These parameters are also listed in Table 1 and the initial CDSDs are shown in Figure 1.

2.3 Model Description

Based on the linear eddy model (*Kerstein*, 1988, 1992), the EMPM is developed to simulate cloud microphysics during entrainment and mixing process (*Krueger et al.*, 1997; *Tölle and Krueger*, 2014; *Su et al.*, 1998). The EMPM predicts the variation of temperature and water vapor fields ranging from the model integral scale to the model Kolmogorov scale (~1 mm). During mixing, the history of droplets in the simulation domain can be tracked. Individual droplets experience different local meteorological environments and then evaporate or grow at different rates (*Su et al.*, 1998). The length, width and height of simulation domain (D) are 20 m, 1 mm and 1 mm, respectively (*Lu et al.*, 2013b; *Luo et al.*, 2020; *Tölle and Krueger*, 2014). Several processes (adiabatic ascent, droplet growth, entrainment, evaporation, and mixing) are involved, which can be explained as follows: Initially, the cloudy parcel containing droplets (the whole domain) adiabatically ascends at a specific rate from the cloud base. Entrainment occurs and the parcel stops to ascend at the entrainment level. Meanwhile, the entrained air randomly replaces a same-sized part of the parcel. Subsequently, molecular diffusion and turbulent deformation occur during the isobaric mixing process at a given turbulence rate. Droplet growth/evaporation is determined by their surrounding environments (*Su et al.*, 1998; *Krueger et al.*, 2008).

The initial CDSDs in Table 1 with different shapes are directly employed for the isobaric mixing without the adiabatic lifting. That is, vertical velocity (w) becomes 0. Note that the configuration is used to study isobaric entrainment-mixing process and is applicable to both lateral and cloud top entrainment-mixing. The simulations are conducted with the turbulent kinetic energy dissipation rate (ε) equal to 5×10^{-3} m^2s^{-3}, the entrained air fraction (f) equal to 0.2 with entrained blob size (l) equal to 2 m (*Tölle and Krueger*, 2014), the entrained dry air relative humidity (RH_e) equal to 82.5%. Sensitivity tests are conducted under different conditions, as shown in Table 2. Each case is performed for 10 realizations with different random number seeds, the same as *Luo et al.* (2020). Only the clouds not completely evaporated after entrainment-mixing are analyzed here with the selection criteria: n_c larger than 10 cm^{-3} and LWC larger than 0.001 g m^{-3} (*Deng et al.*, 2009; *Lu et al.*, 2014b). The simulations that meet the criteria mainly depend on relative humidity, entrained air fraction, and initial liquid water content.

3. Results

3.1 Effects of CDSD Widths on Microphysics during Entrainment-Mixing

Figure 2 shows the temporal evolutions of n_c, LWC, r_v, r_m, σ, and d, when μ equals 0.5, 2.0, 10.0, and 40.0, respectively, in the control run of Table 2. The results are similar for the other conditions listed in Table 2. Both n_c and LWC decrease under all μ conditions. However, for a broader initial CDSD (smaller μ), n_c decreases more significantly because more small droplets are completely evaporated. On the other hand, the decrease in LWC is comparable than n_c for different values of μ, because liquid water needed to evaporate to saturate entrained dry air is mainly determined by the thermodynamic conditions. A narrower CDSD has a slightly faster LWC decrease, because for narrower CDSD, r_m is larger and the phase relaxation time is smaller. The evolution of r_v is more complicated than that of n_c and LWC; r_v increases for the broad initial CDSDs (μ = 0.5, 2.0) but decreases for the narrow ones (μ = 10.0, 40.0). The reason is that the CDSDs with μ = 0.5, 2.0 are mainly composed of small droplets and complete evaporation of small droplets dominates the evaporation (*Luo et al.*, 2020). The remaining big droplets have a larger r_v than the initial CDSDs. On the contrary, for the narrow CDSDs with μ = 10.0, 40.0, partial evaporation of big droplets dominates, which results in a decrease in r_v with time (*Kumar et al.*, 2014; *Tölle and Krueger*, 2014; *Z Gao et al.*, 2018). The variation trend of r_m is similar to that of r_v for each μ. The difference between r_m and r_v is that the initial value of r_m is different for different μ, but r_v is the same.

Intriguingly, σ does not change much during mixing, except for μ = 40.0, suggesting that the change of d is mainly determined by that of r_m rather than σ. Similar to r_m or r_v, the temporal evolution of d is also affected by the competition between complete and partial evaporation. During mixing, d decreases for the initially broad CDSDs with large d (μ = 0.5, 2.0), because of increasing r_m resulting from small droplet complete evaporation (*Pinsky et al.*, 2016; *Luo et al.*, 2020), and nearly unchanged σ. The microphysical features when μ equals 2 are quite similar to those in *Pinsky and Khain*, (2018) and *Pinsky et al.*, (2016) where μ is set to be 3.3 for the broad CDSD. In contrast, for the initially narrow CDSDs (μ = 10.0, 40.0), the CDSDs broaden towards small droplets, attributed to the partial evaporation of big droplets, and thus d increases (*Tölle and Krueger*, 2014).

To further illustrate the effects of initial μ on CDSDs during entrainment-mixing, the evolution of CDSDs is investigated for μ = 40.0 and 0.5, as shown in Figures 3a and 3b. For the initially narrow CDSDs (μ = 40.0), the CDSDs broaden towards small droplets (*Kumar et al.*, 2012, 2014; *Bera et al.*, 2016). The number concentration of big droplets decreases and a tail of small droplets forms, indicating that the CDSDs shift to the left. In contrast, for the initially broad CDSD (μ = 0.5), small droplets drastically decrease, while the big droplets are affected to a lesser extent. Therefore, the proportion of small droplets during mixing decreases for the broad CDSDs and increases for the narrow CDSDs, respectively, as shown in Figures 3c and 3d. In contrast, the proportion of big droplets, respectively, increases and decreases for the broad and narrow CDSDs. It can be also noticed that a long time with minor variations of the CDSDs is needed before reaching new saturation (*Luo et al.*, 2020).

The relationships between d and n_c, r_v, LWC for different CDSD shapes are further examined with more sensitivity tests under different conditions listed in Table 2, including RH_e, ε, and f. In total, 143 out of 216 cases (66.2%) meet the cloud criteria after entrainment-mixing. These factors (RH_e, ε, and f) are reported to have significant effects on microphysical properties and homogeneous mixing degree (*Krueger et al.*, 1997; *Tölle and Krueger*, 2014; *Kumar et al.*, 2014; *Su et al.*, 1998; *Pinsky and Khain*, 2018; *Pinsky et al.*, 2016; *Lu et al.*, 2013b; *Luo et al.*, 2020). For instance, *Lu et al.* (2013b) and *Luo et al*. (2020) showed that the homogeneous mixing degree decreased as f increased, suggesting a larger f caused a smaller homogeneous mixing degree since the complete evaporation of droplets was more likely to occur when the amount of evaporation increased. The microphysical relationships are often used to parameterize d in models (*Peng and Lohmann*, 2003; *Rotstayn and Liu*, 2003, 2009; *Xie and Liu*, 2011; *Xie et al.*, 2017). Figure 4 shows that both the relationship between d and n_c and between d and LWC change from positive to negative as the CDSDs become narrow. For the narrow CDSDs, d increases as n_c and LWC decrease. For the broad CDSDs, d decreases with the decrease of n_c and LWC. The negative relationship between d and n_c for the narrow CDSDs is similar to that in some previous studies (*Ma et al.*, 2010; *Chandrakar et al.*, 2016, 2018; *Lu et al.*, 2012; *Desai et al.*, 2018, 2019) and the positive relationship between d and n_c for the broad CDSDs is similar to other studies (*Martin et al.*, 1994; *Wood*, 2000; *McFarquhar and Heymsfield*, 2001; *Liu and Daum*, 2002; *Yum and Hudson*, 2005; *Pandithurai et al.*, 2012; *Prabha et al.*, 2012; *Anil Kumar et al.*, 2016). It is known that many factors influence the relationship between d and n_c, including vertical velocity, fluctuation of supersaturation, and aerosols (*Liu et al.*, 2006; *Peng et al.*, 2007; *Lu et al.*, 2012; *Hudson et al.*, 2012; *Chandrakar et al.*, 2016). The combination of different factors even produces no correlation between d and n_c (*Zhao et al.*, 2006) or regime-dependent relationships (*Chen et al.*, 2016, 2018). This study adds another layer of complexity: the width of CDSDs itself affects the relationship between d and n_c. Different from the above contrasting relationships, d and r_v are always negatively correlated, but the reasons for this are different between narrow and broad CDSDs. For the narrow CDSDs, d increases and r_v decreases as droplets evaporate whereas d decreases and r_v increases for the broad CDSDs. This result reinforces the argument that the relationship between d and r_v is better than the relationship between d and n_c, in terms of d parameterization (*Wood*, 2000; *Liu et al.*, 2008; *Lu et al.*, 2020).

The microphysical mixing diagrams of the relationships between r_v^3/r_{va}^3 and n_c/n_{ca} and between r_v^3/r_{va}^3 and LWC/LWC$_a$ are further examined (Figure 5) because of their widespread use in studying entrainment-mixing process (*Lu et al.*, 2013b, 2014b). For the narrow CDSDs (μ = 10.0, 40.0), r_v^3/r_{va}^3 decreases during entrainment-mixing, as theoretically expected. However, for the broad CDSDs (μ = 0.5, 2.0), r_v^3/r_{va}^3 increases to be larger than 1.0 with the decreasing n_c/n_{ca} and LWC/LWC$_a$. It is noteworthy that a similar feature has been used for identifying inhomogeneous mixing with subsequent ascent (*Lasher-trapp et al.*, 2005; *Siebert et al.*, 2006; *Lehmann et al.*, 2009; *J Wang et al.*, 2009; *Lu et al.*, 2013a). This physical mechanism is true if CDSDs are narrow. In the concept of inhomogeneous mixing with subsequent ascent, n_c in a cloud parcel decreases due to inhomogeneous mixing; if the parcel goes through subsequent ascent after mixing, the droplets in the parcel grow faster than in adiabatic clouds, because of smaller n_c and weaker competition for water vapor (*Telford*, 1996; *Lasher-trapp et al.*, 2005; *Siebert et al.*, 2006; *Lehmann et al.*, 2009). However, for broad CDSDs, the negative relationships between r_v^3/r_{va}^3 and n_c/n_{ca} and between r_v^3/r_{va}^3 and LWC/LWC$_a$ in Figure 5 do not indicate inhomogeneous mixing with subsequent ascent because isobaric mixing is studied here without updraft. Similarly, assuming a broad CDSD (μ = 3.3), *Pinsky and Khain*, (2018) and *Pinsky et al.*, (2016) also reported that normalized cubic volume-mean radius increased as normalized number concentration decreased, due to the evaporation of small droplets in isobaric mixing.

3.2 New Measures of Homogeneous Mixing Degree

The majority of values of traditional homogeneous mixing degrees (i.e., ψ_j) are negative for the broad CDSDs (Figure 6), which is at odds with the dynamical measures. This inconsistent result suggests that ψ_j are not applicable for the broad CDSDs. Therefore, the influence of the initial CDSD shapes on quantifying homogeneous mixing degrees should be considered. We introduce the new measures of homogeneous mixing degrees, named as bin-weighted homogeneous mixing degrees (ψ_{j_w}, where j is from 1 to 4) in three steps, as illustrated in Figure 7. First, bin the initial CDSD according to the droplet sizes before entrainment-mixing, and then track the history of droplets in individual radius bins during mixing. Second, calculate the homogeneous mixing degrees of the tracked droplets in each radius bin by use of equations (1 - 4), termed as $\psi_{j_{\mathrm{bin}}}$; all the properties in equations (1 - 4) are for each radius bin during entrainment-mixing. Third, average $\psi_{j_{\mathrm{bin}}}$ with the corresponding droplet number concentration (n_{bin}) in each radius bin of instantaneous CDSD for every time step as the weight:

$$\psi_{j_{\mathrm{w}}} = \frac{1}{\sum_{i=1}^{m} n_{bin}(i)} \sum_{i=1}^{m} \psi_{j_{bin}} n_{bin}(i), \tag{6}$$

where m is the number of droplet radius bins; i represents each bin; j is from 1 to 4. The revised definitions are consistent with the notion that the definition of homogeneous mixing degree derived from the conventional diagrams holds for "monodisperse" size distributions. The new measures are further supported by the following three points.

First, the new measures have reasonable ranges of values. The initially monodisperse CDSD before entrainment-mixing is employed to testify the rationality of $\psi_{j_{\mathrm{w}}}$. Figure S1 shows the relationships between $\psi_{j_{\mathrm{w}}}$ and the traditional ψ_j, respectively. Each pair of homogeneous mixing degrees (e.g., the relationship between $\psi_{1_{\mathrm{w}}}$ and ψ_1) shows identical results. Since there is only one initial radius bin, the bin-weighted and traditional homogeneous mixing degrees are equivalent.

The relationships between $\psi_{j_{\mathrm{w}}}$ and the traditional ψ_j are further investigated for different CDSD shapes (μ = 0.5, 2.0, 10.0, 40.0). For these CDSD shapes, the whole droplet radius range is divided into 20 bins according to the droplet sizes within the initial CDSDs. Figure 8 shows that the values of $\psi_{j_{\mathrm{w}}}$ are in the range of 0 – 1.0 for all shapes. As mentioned above, the majority values of ψ_j are negative for μ equal to 0.5

and 2.0, and positive for μ equal to 10.0 and 40.0. When the initial CDSDs are narrow (μ = 10.0, 40.0), ψ_{j_w} are close to ψ_j, respectively, with the data points approaching the 1:1 line. As μ decreases (i.e., the CDSD width increases), the difference between ψ_{j_w} and ψ_j becomes significant, and ψ_{j_w} have a better performance than ψ_j, because ψ_{j_w} are always in the reasonable range of 0 – 1.0. Therefore, it is again confirmed that ψ_j are not proper for the broad CDSDs, in contrast, ψ_{j_w} work for all CDSD shapes.

Second, the new measures are much more consistent with the dynamical measures than old ones. As mentioned above, the homogeneous mixing degrees quantify entrainment-mixing process from the microphysical perspective. It is desirable to use an independent method to verify if the new measures of homogeneous mixing degrees are reasonable. From the dynamical perspective, the Damköhler number (Da) is introduced (*Burnet and Brenguier*, 2007; *Andrejczuk et al.*, 2009):

$$\mathrm{Da} = \frac{\tau_{mix}}{\tau_{evap}}, \quad (7a)$$

$$\tau_{mix} = (L^2/\varepsilon)^{1/3}, \quad (7b)$$

$$\tau_{evap} = -\frac{r_{\mathrm{va}}^{\ 2}}{2AS_{\mathrm{e}}}. \quad (7c)$$

where τ_{mix} is the time scale of turbulent homogenization, τ_{evap} represents the evaporation time, L is the size of a cloud volume; A is related to temperature and pressure (*Rogers and Yau*, 1996); S_e is the dry air supersaturation. Another dynamical property, the transition scale number (N_L), is introduced by *Lu et al.* (2011):

$$N_L = \frac{L^*}{\eta} = \frac{\varepsilon^{1/2}\tau_{\mathrm{evap}}^{\ 3/2}}{\eta}, \quad (8a)$$

$$\eta = (\nu^3/\varepsilon)^{1/4}. \quad (8b)$$

where L^* is the transition length defined by *Lehmann et al.* (2009); η is the Kolmogorov microscale; ν is the kinematic viscosity. A smaller Da or larger N_L indicates a more homogeneous mixing process.

The dynamical parameters Da and N_L are good candidates because they quantify entrainment-mixing process from the dynamical perspective. The relationships of ψ_{j_w} with Da and N_L are the critical indicators that have been used to parameterize different mixing types in atmospheric models (*Lu et al.*, 2018b; *Luo et al.*, 2020; *Z Gao et al.*, 2018). It is well established that Da compares the mixing time scale to evaporation time scale, that is, smaller Da means mixing is faster compared to evaporation, indicating more homogeneous mixing (e.g., *Kumar et al.*, 2013, 2014, 2017); N_L is defined using transition length that is derived by setting Da = 1 (*Lehmann et al.*, 2009; *Lu et al.*, 2011). Homogeneous mixing degrees are expected to be positively correlated with 1/Da and N_L, respectively. With the cases in Table 2, Figures 9 and 10 show that ψ_{j_w} are positively correlated with 1/Da and N_L, respectively, consistent with theoretical expectation and previous results for the narrow CDSDs (*Lu et al.*, 2013b, 2014a, 2018b; *Luo et al.*, 2020; *Z Gao et al.*, 2018). These relationships can be well fitted by

$$y = a\exp(bx^c), \quad (9)$$

where x is 1/Da or N_L; y is ψ_{j_w}; a, b, and c are three fitting parameters. The determination coefficients (R^2) of the relationships between ψ_{j_w} and 1/Da are 0.96, 0.97, 0.98, and 0.98, respectively. The R^2 of the relationships between ψ_{j_w} and N_L are 0.89, 0.92, 0.93, and 0.96, respectively. ψ_j are only weakly correlated with 1/Da and N_L, respectively (see Figures S2 and S3). For example, the correlation coefficients of the relationships between ψ_j and 1/Da are only 0.11, 0.10, 0.10, and 0.10, respectively. Therefore, the rationality of $\psi_{j_{\mathrm{w}}}$, and the irrationality of ψ_j are further confirmed with 1/Da and N_L.

Third, the temporal variation of the new measures has a clear physical explanation. Figure 11 shows the temporal evolution of $\psi_{j_{\mathrm{w}}}$ for μ = 0.5, 2.0, 10.0, and 40.0, respectively. Note that the duration of mixing and evaporation of each simulation in the 10 realizations can be different. To integrate the 10 realizations, the realizations are normalized by their own duration time, respectively, similar to *Luo et al.* (2020). The ensemble mean results are investigated with LWC = 0.5 g m^{-3}, RH_e of 82.5%, ε of 5×10^{-3} m^2s^{-3}, n_d of 119.4 cm^{-3}, and f of 0.2. Generally speaking, the evolutions of $\psi_{j_{\mathrm{w}}}$ are similar; they decrease first and then increase, indicating that the mixing process becomes more inhomogeneous first and then becomes more homogeneous, consistent with *Luo et al*. (2020) and *Krueger et al*. (2008). As suggested by *Broadwell and Breidenthal* (1982), *Jensen and Baker* (1989), and *Krueger et al.*, (1997), there are notable gradients of scalar fields (temperature and water vapor mixing ratio), when dry air is entrained in the beginning of the entrainment-mixing process. Droplets near entrained dry air evaporate significantly or even completely. As a result, $\psi_{j\mathrm{w}}$ decreases. After experiencing significant variation in those scaler fields, they are homogenized. Meanwhile, a long mixing time is needed for the remaining process (mixing between cloud droplets and entrained dry air and also evaporation of cloud droplets) before the model domain is saturated (*Kumar et al.*, 2018). During the relatively long "saturation" process, $\psi_{j_{\mathrm{w}}}$ vary slightly. These characteristics of bin-weighted homogeneous mixing degrees are consistent with those of traditional homogeneous mixing degrees for the narrow CDSDs discussed in *Luo et al.* (2020).

It can be also noticed that the values of ψ_{j_w} generally increase with the increase of μ at the beginning of the simulation and then decrease with the increase of μ at the equilibrium states (i.e., the first time when the averaged relative humidity in the domain is larger than 99.5% (*Lehmann et al*., 2009)). As illustrated in Figures 3c and 3d, the case with μ = 40 has more big droplets with r > 10 μm than small droplets with r < 6 μm at the beginning; the situation is opposite for μ = 0.5. Therefore, partial evaporation is more likely to occur and homogeneous mixing degrees are larger for μ = 40 than for μ = 0.5 at the beginning. The proportion of big droplets decreases for μ = 40 and increases for μ = 0.5 with time. At the equilibrium states, the case with μ = 40 has a smaller proportion of big droplets than that with μ = 0.5 (Figures 3c and 3d). Therefore, homogeneous mixing degrees are smaller for μ = 40 at the equilibrium states. Besides, the broadest CDSDs are the earliest to reach the minimum values of homogeneous mixing degrees, since the small droplets dominate the broad CDSDs, and the complete evaporation time of small droplets should be the shortest.

Several sensitivity tests are carried out to test the robustness of the above results, including the droplet number concentration, the liquid water content, the entrained blob size, the weight functions, and the number of bins. The sensitivity tests of n_d are conducted with n_d equal to 69.1, 119.4, and 233.1 cm^{-3}, which correspond to r_v equal to 12, 10, and 8 μm, respectively. The other model input parameters are the same as those in Figure 2. There, LWC is equal to 0.5 g m^{-3}, RH$_e$ is equal to 82.5%, f is equal to 0.2, and ε is equal to 5×10^{-3} m^{2}s^{-3}. Figures S4 and S5 (see the Supporting Information) show the performance of ψ_{j_w} when μ equals 0.5 and 40, respectively. Generally speaking, the tendencies of ψ_{j_w} are similar under different n_d conditions. The higher n_d causes the smaller values of ψ_{j_w} since the higher n_d corresponds to the smaller droplet size and complete evaporation is more significant.

Similarly, LWC equal to 0.1, 0.5 and 1.0 g m^{-3} is employed to test the sensitivity of LWC. However, when LWC = 0.1 g m^{-3}, cloud completely dissipates after entrainment-mixing. Therefore, the results with LWC equal to 0.5 and 1.0 g m^{-3} are shown in Figures S6 and S7. For the both broad and narrow CDSDs, the tendencies of ψ_{j_w} are similar for different LWC values. When $\mu = 0.5$, the higher LWC has smaller values of ψ_{j_w} at the equilibrium states; the reason is that the higher LWC has more small droplets than big droplets and complete evaporation of small droplets dominates. In contrast, when $\mu = 40.0$, the higher LWC has more big droplets than small droplets; therefore, partial evaporation dominates, and ψ_{j_w} at equilibrium states are larger for the higher LWC.

The sensitivity tests of l (i.e., entrained blob size) are carried out when l equals 0.5, 1, 2 and 4 m, respectively, keeping the entrained air fraction equal to 0.2 (Figures S8 and S9). For both the broad CDSD ($\mu = 0.5$) and narrow CDSD ($\mu = 40$), the results are generally similar for different l. As theoretically expected, the mixing time scale is smaller for smaller l, therefore, the entrainment-mixing mechanism is more homogeneous, i.e., the larger bin-weighted homogeneous mixing degrees.

The surface area, the liquid water content, and the radar reflectivity factor are taken as the weights to calculate ψ_{j_w}, respectively. These weights correspond to the second, third, and sixth moments of radius, respectively. The weight of number concentration is the zeroth moment. As shown in Figures S10 - S12, the temporal evolution of ψ_{j_w} is similar to those in Figure 11; the relationships between ψ_{j_w} and ψ_j are also similar to those in Figure 8. However, a higher moment weight causes narrower ranges of ψ_{j_w} than a lower moment weight, which means that ψ_{j_w} of a higher moment weight have smaller ranges of temporal variation. Furthermore, for the narrow CDSD ($\mu = 40$), it is expected to see the data points of the relationship between ψ_{j_w} and ψ_j fall along the 1:1 line. However, the data points deviate from the 1:1 line more and more significantly as the weight moment increases. Therefore, it is also good to use other weights (e.g., the surface area, the liquid water content, and the radar reflectivity factor), but number concentration is recommended.

The sensitivity tests of number of bins are performed with the different number of bins: 1, 5, 10, 20, 30, and 50 (Figures S13 - S16). Since homogeneous/inhomogeneous mixing is a “bulk” concept, the number of droplets in each bin need to be statistically large enough to calculate the bin-weighted homogeneous mixing degrees. When the number of bins is 1, the results are the traditional homogeneous mixing degrees, and some values are unrealistically negative. For the number of bins equal to 5, the bin-weighted homogeneous mixing degrees become positive. As the number of bins increases to 20 or larger, the bin-weighted homogeneous mixing degrees are not sensitive to the number of bins. Therefore, the bin number of 20 is recommended here.

4. Conclusions and Discussions

This study first qualitatively presents the microphysical properties and entrainment-mixing mechanism for CDSDs with different widths using the Explicit Mixing Parcel Model. Then traditional homogeneous mixing degrees are analyzed and new measures for quantifying entrainment-mixing mechanism are defined. The main results are summarized below.

First, the temporal evolution of microphysical properties indicates that, for both initially narrow and broad CDSDs, liquid water content and droplet number concentration decrease. However, the volume-mean radius and mean radius increase for the broad CDSDs and decrease for the narrow ones. Relative dispersion of CDSDs decreases for the broad CDSDs and increases for the narrow ones, which can be attributed to the variation of mean radius rather than that of standard deviation, since standard deviation only changes slightly during mixing. Further analyses with the evolution of CDSDs indicate that complete evaporation dominates for the broad CDSDs because there are many small droplets; partial evaporation dominates for the narrow CDSDs, which broadens the CDSDs towards the small droplets.

Second, besides temporal evolution, the relationships of microphysics show that relative dispersion is positively correlated with liquid water content and number concentration for the broad CDSDs; the correlations become negative as the CDSDs become narrow. Many factors have been found to affect the sign of the correlation of relative dispersion versus number concentration, e.g., vertical velocity, fluctuation of supersaturation, and aerosols (*Hudson et al.*, 2012; *Peng et al.*, 2007; *Liu et al.*, 2006; *Chandrakar et al.*, 2016; *Lu et al.*, 2012). The spectral width is found to be an important factor. Different from the above two relationships, relative dispersion and volume-mean radius are always negatively correlated. Volume-mean radius is positively correlated with both liquid water content and number concentration for the narrow CDSDs, but negatively correlated with the two quantities for the broad CDSDs, which could be mistaken as inhomogeneous mixing with subsequent ascent. The traditional homogeneous mixing degrees defined based on the above two relationships are negative for the broad CDSDs, indicating the limitation of the traditional measures.

Third, to overcome the above limitation, new measures of homogeneous mixing degrees considering the CDSD shapes are introduced and named as bin-weighted homogeneous mixing degrees. This method measures the homogeneity of entrainment-mixing process by binning the initial CDSD according to the droplet sizes and averaging the homogeneous mixing degree in individual radius bin with the corresponding number concentration in each radius bin of instantaneous CDSD for every time step as the weight. Three arguments supporting the rationality of the new method are provided. First, the bin-weighted homogeneous mixing degrees are always in the range of 0 – 1.0 for different CDSDs widths and are exactly the same as the traditional homogeneous mixing degrees when the CDSDs narrow to monodisperse. Second, the bin-weighted homogeneous mixing degrees are positively correlated with reciprocal of Damköhler number and transitional scale number, which is consistent with theoretical expectation and previous results (*Lu et al.*, 2013b, 2014a, 2018b; *Luo et al.*, 2020; *Z Gao et al.*, 2018). Third, the new measures decrease first and then increase during mixing for both narrow and broad CDSDs; the difference of the bin-weighted homogeneous mixing degrees between the simulations with the narrow and broad CDSDs can also be well explained physically.

It is noteworthy that defining discrete bin-weighted homogeneous mixing degrees could be the first step to quantitatively represent entrainment-mixing mechanism considering cloud spectral width. In future studies, it would be better to define a continuous version of homogeneous mixing degree including relative dispersion or the shape parameter in the gamma distribution.

Acknowledgments

We thank Sinan Gao and Zhuangzhuang Zhou in NUIST for helpful discussions. We also appreciate three reviewers for their valuable suggestions/comments and Mr. Brandon J Bethel for editing. This research is supported by the National Key Research and Development Program of China (2019YFA0606803), the Second Tibetan Plateau Scientific Expedition and Research (STEP) program (2019QZKK0105), the National Natural Science Foundation of China (41822504, 42027804, 42075073, 41975181), and the National Center of Meteorology, Abu Dhabi, UAE under the UAE Research Program for Rain Enhancement Science. Liu is supported by the U.S. Department of Energy Atmospheric System Research (ASR) Program (DE-SC00112704) and Solar Energy Technologies Office (SETO) under Award 33504. The simulation data are published in http://dx.doi.org/10.17632/wc8c7wcyjb.1.

Caption List

Figure 1. The initial CDSDs for different shape parameters (μ) in Table 1, with droplet number concentration of 119.4 cm^{-3}, volume-mean radius of 10.0 μm and liquid water content of 0.5 g m^{-3}.

Figure 2. Temporal evolutions of (a) number concentration (n_c), (b) liquid water content (LWC), (c) volume-mean radius (r_v), (d) mean radius (r_m), (e) standard deviation (σ), and (f) relative dispersion (d) for different cloud droplet size distribution shape parameters (μ). The model input parameters are shown in the control run of Table 2.

Figure 3. (a) and (b) Temporal evolution of CDSDs with their shape parameters (μ) equal to 40.0 and 0.5, respectively. (c) and (d) Temporal evolution of the ratios of big and small droplet number concentrations to the total droplet number concentration, respectively. The criteria for big and small droplets are radius (r) larger than 10 μm and smaller than 6 μm, respectively, which are shown as the vertical dash lines. The model input parameters are shown in the control run of Table 2.

Figure 4. Relationships between relative dispersion (d) and number concentration (n_c), volume-mean radius (r_v), and liquid water content (LWC) for different cloud droplet size distribution shape parameters (μ) as listed in Table 2.

Figure 5. (a) Relationship between r_v^3/r_{va}^3 and n_c/n_a, and (b) relationship between r_v^3/r_{va}^3 and LWC/LWC$_a$ for different cloud droplet size distribution shape parameters (μ). The time direction is represented by the four arrows. The model input parameters are shown in the control run of Table 2.

Figure 6. Temporal evolutions of traditional homogeneous mixing degrees (ψ_1, ψ_2, ψ_3, ψ_4) for different cloud droplet size distribution shape parameters (μ). The model input parameters are shown in the control run of Table 2.

Figure 7. Schematic for defining the bin-weighted homogeneous mixing degree. The blue CDSD represents an instantaneous CDSD during entrainment-mixing for every time step. Number concentration (n_{bin}) and homogeneous mixing degree (ψ_{bin}) of the droplets in each radius bin are used to calculate the bin-weighted homogeneous mixing degree. The radius bins are divided according to the initial CDSD. See text for the detailed explanation.

Figure 8. Relationships between bin-weighted homogeneous mixing degrees (${\psi_1}_w$, ${\psi_2}_w$, ${\psi_3}_w$, ${\psi_4}_w$) and traditional homogeneous mixing degrees (ψ_1, ψ_2, ψ_3, ψ_4) for different cloud droplet size distributions with the shape parameters (μ) equal to 0.5, 2.0, 10.0, and 40.0. The model input parameters are shown in the control run of Table 2.

Figure 9. Joint probability density functions (PDFs) of the relationships between bin-

weighted homogeneous mixing degrees and the reciprocal of Damköhler number (1/Da) of all simulated cases in Table 2. The mean values of bin-weighted homogeneous mixing degrees (diamond data points) are fitted with R^2 and p-value representing the determination coefficient and significance level, respectively. The standard deviations of bin-weighted homogeneous mixing degrees are shown as the error bars.

Figure 10. Same as Figure 9 but for N_L.

Figure 11. Temporal evolutions of bin-weighted homogeneous mixing degrees for different cloud droplet size distribution shape parameters (μ). The model input parameters are shown in the control run of Table 2.

References

Ackerman, A. S., Kirkpatrick, M. P., Stevens, D. E., & Toon, O. B. (2004). The impact of humidity above stratiform clouds on indirect aerosol climate forcing. *Nature*, *432*(7020), 1014-1017. 10.1038/nature03174

Andrejczuk, M., Grabowski, W. W., Malinowski, S. P., & Smolarkiewicz, P. K. (2009). Numerical simulation of cloud–clear air interfacial mixing: Homogeneous versus inhomogeneous mixing. *Journal of the Atmospheric Sciences*, *66*(8), 2493-2500.

Anil Kumar, V., Pandithurai, G., Leena, P. P., Dani, K. K., Murugavel, P., Sonbawne, S. M., et al. (2016). Investigation of aerosol indirect effects on monsoon clouds using ground-based measurements over a high-altitude site in Western Ghats. *Atmospheric Chemistry and Physics*, *16*(13), 8423-8430.

Baker, M., Corbin, R., & Latham, J. (1980). The influence of entrainment on the evolution of cloud droplet spectra: I. A model of inhomogeneous mixing. *Quarterly Journal of the Royal Meteorological Society*, *106*(449), 581-598.

Beals, M. J., Fugal, J. P., Shaw, R. A., Lu, J., Spuler, S. M., & Stith, J. L. (2015). Holographic measurements of inhomogeneous cloud mixing at the centimeter scale. *Science*, *350*(6256), 87-90. 10.1126/science.aab0751

Beard, K. V., & Ochs, H. (1993). Warm-rain initiation: An overview of microphysical mechanisms. *Journal of Applied Meteorology*, *32*(4), 608-625.

Bera, S., Prabha, T. V., & Grabowski, W. W. (2016). Observations of monsoon convective cloud microphysics over India and role of entrainment□mixing. *Journal of Geophysical Research: Atmospheres*, *121*(16), 9767-9788.

Burnet, F., & Brenguier, J.-L. (2007). Observational study of the entrainment-mixing process in warm convective clouds. *Journal of the Atmospheric Sciences*, *64*(6), 1995-2011. 10.1175/jas3928.1

Chandrakar, K. K., Cantrell, W., Chang, K., Ciochetto, D., Niedermeier, D., Ovchinnikov, M., et al. (2016). Aerosol indirect effect from turbulence-induced broadening of cloud-droplet size distributions. *Proceedings of the National Academy of Sciences*, *113*(50), 14243-14248.

Chandrakar, K. K., Cantrell, W., & Shaw, R. A. (2018). Influence of Turbulent Fluctuations on Cloud Droplet Size Dispersion and Aerosol Indirect Effects. *Journal of the Atmospheric Sciences*, *75*(9), 3191-3209. 10.1175/jas-d-18-0006.1

Chandrakar, K. K., Saito, I., Yang, F., Cantrell, W., Gotoh, T., & Shaw, R. A. (2020). Droplet size distributions in turbulent clouds: experimental evaluation of theoretical distributions. *Quarterly Journal of the Royal Meteorological Society*, *146*(726), 483-504.

Chen, J., Liu, Y., Zhang, M., & Peng, Y. (2016). New understanding and quantification of the regime dependence of aerosol□cloud interaction for studying aerosol indirect effects. *Geophysical Research Letters*, *43*(4), 1780-1787.

Chen, J., Liu, Y., Zhang, M., & Peng, Y. (2018). Height Dependency of Aerosol-Cloud Interaction Regimes. *Journal of Geophysical Research: Atmospheres*, *123*(1), 491-506. 10.1002/2017jd027431

Cooper, W. A., Lasher-Trapp, S. G., & Blyth, A. M. (2013). The Influence of Entrainment and Mixing on the Initial Formation of Rain in a Warm Cumulus

Cloud. *Journal of the Atmospheric Sciences*, *70*(6), 1727-1743. 10.1175/jas-d-12-0128.1

Del Genio, A. D., & Wu, J. (2010). The role of entrainment in the diurnal cycle of continental convection. *Journal of Climate*, *23*(10), 2722-2738.

Del Genio, A. D., Wu, J., Wolf, A. B., Chen, Y., Yao, M.-S., & Kim, D. (2015). Constraints on Cumulus Parameterization from Simulations of Observed MJO Events. *Journal of Climate*, *28*(16), 6419-6442. 10.1175/jcli-d-14-00832.1

Deng, Z., Zhao, C., Zhang, Q., Huang, M., & Ma, X. (2009). Statistical analysis of microphysical properties and the parameterization of effective radius of warm clouds in Beijing area. *Atmospheric research*, *93*(4), 888-896. 10.1016/j.atmosres.2009.04.011

Desai, N., Chandrakar, K. K., Chang, K., Cantrell, W., & Shaw, R. A. (2018). Influence of Microphysical Variability on Stochastic Condensation in a Turbulent Laboratory Cloud. *Journal of the Atmospheric Sciences*, *75*(1), 189-201. 10.1175/jas-d-17-0158.1

Desai, N., Glienke, S., Fugal, J., & Shaw, R. A. (2019). Search for Microphysical Signatures of Stochastic Condensation in Marine Boundary Layer Clouds Using Airborne Digital Holography. *Journal of Geophysical Research: Atmospheres*, *124*(5), 2739-2752. 10.1029/2018jd029033

Donner, L. J., O'Brien, T. A., Rieger, D., Vogel, B., & Cooke, W. F. (2016). Are atmospheric updrafts a key to unlocking climate forcing and sensitivity? *Atmospheric Chemistry and Physics*, *16*(20), 12983-12992. 10.5194/acp-16-

12983-2016

Feingold, G., Cotton, W. R., Kreidenweis, S. M., & Davis, J. T. (1999). The Impact of Giant Cloud Condensation Nuclei on Drizzle Formation in Stratocumulus: Implications for Cloud Radiative Properties. *Journal of the Atmospheric Sciences*, *56*(24), 4100-4117. 10.1175/1520-0469(1999)056<4100:tiogcc>2.0.co;2

Freud, E., Rosenfeld, D., & Kulkarni, J. R. (2011). Resolving both entrainment-mixing and number of activated CCN in deep convective clouds. *Atmospheric Chemistry and Physics*, *11*(24), 12887-12900. 10.5194/acp-11-12887-2011

Gao, S., Lu, C., Liu, Y., Mei, F., Wang, J., Zhu, L., & Yan, S. (2020). Contrasting Scale Dependence of Entrainment□Mixing Mechanisms in Stratocumulus Clouds. *Geophysical Research Letters*, e2020GL086970. 10.1029/2020GL086970

Gao, W., Sui, C., Fan, J., Hu, Z., & Zhong, L. (2016). A study of cloud microphysics and precipitation over the Tibetan Plateau by radar observations and cloud□resolving model simulations. *Journal of Geophysical Research*, *121*(22), 13752.

Gao, Z., Liu, Y., Li, X., & Lu, C. (2018). Investigation of turbulent entrainment□mixing processes with a new particle□resolved direct numerical simulation model. *Journal of Geophysical Research: Atmospheres*, *123*(4), 2194-2214.

Gerber, H. E., Frick, G. M., Jensen, J. B., & Hudson, J. G. (2008). Entrainment, mixing, and microphysics in trade-wind cumulus. *Journal of the Meteorological Society of Japan. Ser. II*, *86*, 87-106.

Grabowski, W. W. (2006). Indirect Impact of Atmospheric Aerosols in Idealized Simulations of Convective–Radiative Quasi Equilibrium. *Journal of Climate*, *19*(18), 4664-4682. 10.1175/jcli3857.1

Guo, J., Su, T., Chen, D., Wang, J., Li, Z., Lv, Y., et al. (2019). Declining summertime local‐scale precipitation frequency over China and the United States, 1981–2012: The disparate roles of aerosols. *Geophysical Research Letters*, *46*(22), 13281-13289.

Haman, K. E., Malinowski, S. P., Kurowski, M. J., Gerber, H., & Brenguier, J.-L. (2007). Small scale mixing processes at the top of a marine stratocumulus—a case study. *Quarterly Journal of the Royal Meteorological Society*, *133*(622), 213-226. 10.1002/qj.5

Hill, A. A., Feingold, G., & Jiang, H. (2009). The Influence of Entrainment and Mixing Assumption on Aerosol–Cloud Interactions in Marine Stratocumulus. *Journal of the Atmospheric Sciences*, *66*(5), 1450-1464. 10.1175/2008jas2909.1

Hoffmann, F., & Feingold, G. (2019). Entrainment and Mixing in Stratocumulus: Effects of a New Explicit Subgrid-Scale Scheme for Large-Eddy Simulations with Particle-Based Microphysics. *Journal of the Atmospheric Sciences*, *76*(7), 1955-1973.

Hudson, J. G., Noble, S., & Jha, V. (2012). Cloud droplet spectral width relationship to CCN spectra and vertical velocity. *Journal of Geophysical Research: Atmospheres*, *117*(D11), n/a-n/a. 10.1029/2012jd017546

Jarecka, D., Grabowski, W. W., Morrison, H., & Pawlowska, H. (2013). Homogeneity of the subgrid-scale turbulent mixing in large-eddy simulation of shallow convection. *Journal of the Atmospheric Sciences*, *70*(9), 2751-2767.

Jensen, J. B., Austin, P., Baker, M., & Blyth, A. (1985). Turbulent mixing, spectral evolution and dynamics in a warm cumulus cloud. *Journal of the Atmospheric Sciences*, *42*(2), 173-192.

Johnson, D. B. (1982). The Role of Giant and Ultragiant Aerosol Particles in Warm Rain Initiation. *Journal of the Atmospheric Sciences*, *39*(2), 448-460. 10.1175/1520-0469(1982)039<0448:trogau>2.0.co;2

Kerstein, A. R. (1988). A linear-eddy model of turbulent scalar transport and mixing. *Combustion Science and Technology*, *60*(4-6), 391-421.

Kerstein, A. R. (1992). Linear-eddy modelling of turbulent transport. Part 7. Finite-rate chemistry and multi-stream mixing. *Journal of Fluid Mechanics*, *240*, 289-313.

Kim, B. G., Miller, M. A., Schwartz, S. E., Liu, Y., & Min, Q. (2008). The role of adiabaticity in the aerosol first indirect effect. *Journal of Geophysical Research: Atmospheres*, *113*(D5). 10.1029/2007JD008961

Krueger, S. K., Schlueter, H., & Lehr, P. (2008), Fine-scale modeling of entrainment and mixing of cloudy and clear air, paper presented at 15th International Conference on Clouds and Precipitation, Cancun, Mexico.

Krueger, S. K., Su, C.-W., & McMurtry, P. A. (1997). Modeling entrainment and finescale mixing in cumulus clouds. *Journal of the Atmospheric Sciences*, *54*(23), 2697-2712. doi:10.1175/1520-0469(1997)054<2697:MEAFMI>2.0.CO;2

Kumar, B., Götzfried, P., Suresh, N., Schumacher, J., & Shaw, R. A. (2018). Scale Dependence of Cloud Microphysical Response to Turbulent Entrainment and Mixing. *Journal of Advances in Modeling Earth Systems*, *10*(11), 2777-2785.

Kumar, B., Janetzko, F., Schumacher, J., & Shaw, R. (2012). extreme response of a coupled scalar-particle system during turbulent mixing. *New Journal of Physics*

Kumar, B., Schumacher, J., & Shaw, R. A. (2013). Cloud microphysical effects of turbulent mixing and entrainment. *Theoretical and Computational Fluid Dynamics*, *27*(3-4), 361-376. 10.1007/s00162-012-0272-z

Kumar, B., Schumacher, J., & Shaw, R. A. (2014). Lagrangian mixing dynamics at the cloudy–clear air interface. *Journal of the Atmospheric Sciences*, *71*(7), 2564-2580. 10.1175/JAS-D-13-0294.1

Lasher-trapp, S. G., Cooper, W. A., & Blyth, A. M. (2005). Broadening of droplet size distributions from entrainment and mixing in a cumulus cloud. *Quarterly Journal of the Royal Meteorological Society*, *131*(605), 195-220. 10.1256/qj.03.199

Lehmann, K., Siebert, H., & Shaw, R. A. (2009). Homogeneous and inhomogeneous mixing in cumulus clouds: Dependence on local turbulence structure. *Journal of the Atmospheric Sciences*, *66*(12), 3641-3659. 10.1175/2009jas3012.1

Li, J., Chen, J., Lu, C., & Wu, X. (2020). Impacts of TIPEX□III Rawinsondes on the Dynamics and Thermodynamics Over the Eastern Tibetan Plateau in the Boreal Summer. *Journal of Geophysical Research: Atmospheres*, *125*(13), e2020JD032635. 10.1029/2020JD032635

Lin, Y., Huang, X., Liang, Y., Qin, Y., Xu, S., Huang, W., et al. (2020). Community Integrated Earth System Model (CIESM): Description and Evaluation. *Journal of Advances in Modeling Earth Systems*, *12*(8) 10.1029/2019ms002036

Liu, Y. (2019). Introduction to the Special Section on Fast Physics in Climate Models:

Parameterization, Evaluation, and Observation. *Journal of Geophysical Research: Atmospheres* 10.1029/2019jd030422

Liu, Y., Daum, P., Guo, H., & Peng, Y. (2008). Dispersion bias, dispersion effect, and the aerosol–cloud conundrum. *Environmental Research Letters*, *3*, 045021.

Liu, Y., & Daum, P. H. (2002). Anthropogenic aerosols: Indirect warming effect from dispersion forcing. *Nature*, *419*(6907), 580-581.

Liu, Y., Daum, P. H., Chai, S. K., & Liu, F. (2002), Cloud parameterizations,cloud physics, and their connections: An overview *Rep.*, Brookhaven National Lab., Upton, NY (US).

Liu, Y., Daum, P. H., & Yum, S. S. (2006). Analytical expression for the relative dispersion of the cloud droplet size distribution. *Geophysical Research Letters*, *33*(2). 10.1029/2005GL024052

Liu, Y., Laiguang, Y., Weinong, Y., & Feng, L. (1995). On the size distribution of cloud droplets. *Atmospheric research*, *35*(2-4), 201-216.

Lu, C., Liu, Y., & Niu, S. (2011). Examination of turbulent entrainment-mixing mechanisms using a combined approach. *Journal of Geophysical Research*, *116*(D20) 10.1029/2011jd015944

Lu, C., Liu, Y., & Niu, S. (2013a). A method for distinguishing and linking turbulent entrainment mixing and collision-coalescence in stratocumulus clouds. *Chinese science bulletin*, *58*(4-5), 545-551. 10.1007/s11434-012-5556-6

Lu, C., Liu, Y., & Niu, S. (2014a). Entrainment-mixing parameterization in shallow cumuli and effects of secondary mixing events. *Chinese science bulletin*, *59*(9), 896-903.

Lu, C., Liu, Y., Niu, S., & Endo, S. (2014b). Scale dependence of entrainment□mixing mechanisms in cumulus clouds. *Journal of Geophysical Research Atmospheres*, *119*(24), 13.

Lu, C., Liu, Y., Niu, S., Krueger, S., & Wagner, T. (2013b). Exploring parameterization for turbulent entrainment-mixing processes in clouds. *Journal of Geophysical Research: Atmospheres*, *118*(1), 185-194. 10.1029/2012jd018464

Lu, C., Liu, Y., Niu, S., & Vogelmann, A. M. (2012). Observed impacts of vertical velocity on cloud microphysics and implications for aerosol indirect effects. *Geophysical Research Letters*, *39*(21), n/a-n/a. 10.1029/2012gl053599

Lu, C., Liu, Y., Niu, S., & Xue, Y. (2018a). Broadening of cloud droplet size distributions and warm rain initiation associated with turbulence: an overview. *Atmospheric and Oceanic Science Letters*, *11*(2), 123-135.

Lu, C., Liu, Y., Yum, S. S., Chen, J., Zhu, L., Gao, S., et al. (2020). Reconciling Contrasting Relationships Between Relative Dispersion and Volume□Mean Radius of Cloud Droplet Size Distributions. *Journal of Geophysical Research: Atmospheres*, *125*(9), e2019JD031868. 10.1029/2019JD031868

Lu, C., Liu, Y., Zhu, B., Yum, S. S., Krueger, S. K., Qiu, Y., et al. (2018b). On which microphysical time scales to use in studies of entrainment□mixing mechanisms in clouds. *Journal of Geophysical Research: Atmospheres*, *123*(7), 3740-3756.

Lu, C., Niu, S., Liu, Y., & Vogelmann, A. M. (2013c). Empirical relationship between entrainment rate and microphysics in cumulus clouds. *Geophysical Research*

Letters, *40*(10), 2333-2338. 10.1002/grl.50445

Luo, S., Lu, C., Liu, Y., Bian, J., Gao, W., Li, J., et al. (2020). Parameterizations of Entrainment□Mixing Mechanisms and Their Effects on Cloud Droplet Spectral Width Based on Numerical Simulations. *Journal of Geophysical Research: Atmospheres*, *125*(22). 10.1029/2020jd032972

Ma, J., Chen, Y., Wang, W., Yan, P., Liu, H., Yang, S., et al. (2010). Strong air pollution causes widespread haze-clouds over China. *Journal of Geophysical Research: Atmospheres*, *115*(D18), D18204. 10.1029/2009jd013065

Martin, G. M., Johnson, D. W., & Spice, A. (1994). The measurement and parameterization of effective radius of droplets in warm stratocumulus clouds. *Journal of the Atmospheric Sciences*, *51*(13), 1823-1842. doi:10.1175/1520-0469(1994)051<1823:TMAPOE>2.0.CO;2

McFarquhar, G. M., & Heymsfield, A. J. (2001). Parameterizations of INDOEX microphysical measurements and calculations of cloud susceptibility: Applications for climate studies. *Journal of Geophysical Research: Atmosphere*, *106*(D22), 28675-28698.

McFarquhar, G. M., Hsieh, T.-L., Freer, M., Mascio, J., & Jewett, B. F. (2015). The Characterization of Ice Hydrometeor Gamma Size Distributions as Volumes in N0–λ–μ Phase Space: Implications for Microphysical Process Modeling. *Journal of the Atmospheric Sciences*, *72*(2), 892-909. 10.1175/jas-d-14-0011.1

McGraw, R., & Liu, Y. (2006). Brownian drift-diffusion model for evolution of droplet size distributions in turbulent clouds. *Geophysical Research Letters*, *33*(3)

10.1029/2005gl023545

Morrison, H., & Grabowski, W. W. (2008). Modeling supersaturation and subgrid-scale mixing with two-moment bulk warm microphysics. *Journal of the Atmospheric Sciences*, *65*(3), 792-812. doi:10.1175/2007JAS2374.1

Pandithurai, G., Dipu, S., Prabha, T. V., Maheskumar, R. S., Kulkarni, J. R., & Goswami, B. N. (2012). Aerosol effect on droplet spectral dispersion in warm continental cumuli. *Journal of Geophysical Research: Atmosphere*, *117*(D16), D16202.

Pawlowska, H., & Brenguier, J.-L. (2000). Microphysical properties of stratocumulus clouds during ACE-2. *Tellus B*, *52*(2), 868-887. 10.1034/j.1600-0889.2000.00076.x

Peng, Y., & Lohmann, U. (2003). Sensitivity study of the spectral dispersion of the cloud droplet size distribution on the indirect aerosol effect. *Geophysical Research Letters*, *30*(10), 1507. 10.1029/2003gl017192

Peng, Y., Lohmann, U., Leaitch, R., & Kulmala, M. (2007). An investigation into the aerosol dispersion effect through the activation process in marine stratus clouds. *Journal of Geophysical Research: Atmosphere*, *112*. 10.1029/2006JD007401

Pinsky, M., Khain, A., Korolev, A., & Magaritz-Ronen, L. (2016). Theoretical investigation of mixing in warm clouds–Part 2: Homogeneous mixing. *Atmospheric Chemistry and Physics*, *16*(14), 9255-9272.

Pinsky, M., & Khain, A. (2018). Theoretical analysis of mixing in liquid clouds–Part IV: DSD evolution and mixing diagrams. *Atmospheric Chemistry and Physics*, *18*(5), 3659-3676.

Prabha, T. V., Patade, S., Pandithurai, G., Khain, A., Axisa, D., Pradeep-Kumar, P., et al. (2012). Spectral width of premonsoon and monsoon clouds over Indo-Gangetic valley. *Journal of Geophysical Research: Atmosphere*, *117*(D20), D20205. 10.1029/2011JD016837

Prabhakaran, P., Shawon, A. S. M., Kinney, G., Thomas, S., Cantrell, W., & Shaw, R. A. (2020). The role of turbulent fluctuations in aerosol activation and cloud formation. *Proceedings of the National Academy of Sciences*, *117*(29), 16831-16838.

Randall, D. A., Bitz, C. M., Danabasoglu, G., Denning, A. S., Gent, P. R., Gettelman, A., et al. (2019a). 100 Years of Earth System Model Development. *Meteorological Monographs*, *59*, 12.11-12.66. 10.1175/amsmonographs-d-18-0018.1

Randall, D. A., Srinivasan, J., Nanjundiah, R. S., & Mukhopadhyay, P. (2019b). *Current trends in the representation of physical processes in weather and climate models.* Springer.

Rogers, R., & Yau, M. K. (1996). *A short course in cloud physics.* Elsevier.

Rotstayn, L. D., & Liu, Y. (2003). Sensitivity of the first indirect aerosol effect to an increase of cloud droplet spectral dispersion with droplet number concentration. *Journal of Climate*, *16*(21), 3476-3481.

Rotstayn, L. D., & Liu, Y. (2009). Cloud droplet spectral dispersion and the indirect aerosol effect: Comparison of two treatments in a GCM. *Geophysical Research Letters*, *36*(10) 10.1029/2009gl038216

Siebert, H., Franke, H., Lehmann, K., Maser, R., Saw, E. W., Schell, D., et al. (2006). Probing finescale dynamics and microphysics of clouds with helicopter-borne measurements. *Bulletin of the American Meteorological Society*, *87*(12), 1727-1738.

Small, J. D., & Chuang, P. Y. (2008). New Observations of Precipitation Initiation in Warm Cumulus Clouds. *Journal of the Atmospheric Sciences*, *65*(9), 2972-2982. doi:10.1175/2008JAS2600.1

Su, C.-W., Krueger, S. K., McMurtry, P. A., & Austin, P. H. (1998). Linear eddy modeling of droplet spectral evolution during entrainment and mixing in cumulus clouds. *Atmospheric research*, 41-58.

Telford, J. (1996), Clouds with turbulence; the role of entrainment, Atmospheric research, *40*(2-4), 261-282.

Tölle, M. H., & Krueger, S. K. (2014). Effects of entrainment and mixing on droplet size distributions in warm cumulus clouds. *Journal of Advances in Modeling Earth Systems*, *6*(2), 281-299.

Wang, J., Daum, P. H., Yum, S. S., Liu, Y., Senum, G. I., Lu, M. L., et al. (2009). Observations of marine stratocumulus microphysics and implications for processes controlling droplet spectra: Results from the Marine Stratus/Stratocumulus Experiment. *Journal of Geophysical Research: Atmospheres*, *114*(D18). 10.1029/2008JD011035

Wang, Y., Fan, J., Zhang, R., Leung, L. R., & Franklin, C. (2013). Improving bulk microphysics parameterizations in simulations of aerosol effects. *Journal of*

Geophysical Research: Atmospheres, *118*(11), 5361-5379.

Wood, R. (2000). Parametrization of the effect of drizzle upon the droplet effective radius in stratocumulus clouds. *Quarterly Journal of the Royal Meteorological Society*, *126*(570), 3309-3324. 10.1002/qj.49712657015

Wood, R. (2012). Stratocumulus Clouds. *Monthly Weather Review*, *140*(8), 2373-2423. 10.1175/mwr-d-11-00121.1

Wu, W., & McFarquhar, G. M. (2018). Statistical Theory on the Functional Form of Cloud Particle Size Distributions. *Journal of the Atmospheric Sciences*, *75*(8), 2801-2814. 10.1175/jas-d-17-0164.1

Xie, X., & Liu, X. (2011). Effects of spectral dispersion on clouds and precipitation in mesoscale convective systems. *Journal of Geophysical Research: Atmospheres*, *116*(D6) 10.1029/2010jd014598

Xie, X., Zhang, H., Liu, X., Peng, Y., & Liu, Y. (2017). Sensitivity study of cloud parameterizations with relative dispersion in CAM5.1: impacts on aerosol indirect effects. *Atmospheric Chemistry and Physics*, *17*(9), 5877-5892. 10.5194/acp-17-5877-2017

Xu, X., Lu, C., Liu, Y., Gao, W., Wang, Y., Cheng, Y., et al. (2020). Effects of Cloud Liquid□Phase Microphysical Processes in Mixed□Phase Cumuli Over the Tibetan Plateau. *Journal of Geophysical Research: Atmospheres*, *125*(19) 10.1029/2020jd033371

Xu, X., & Xue, H. (2015). Impacts of Free-Tropospheric Temperature and Humidity on Nocturnal Nonprecipitating Marine Stratocumulus. *Journal of the Atmospheric*

Sciences, *72*(8), 2853-2864. 10.1175/jas-d-14-0387.1

Xue, H., & Feingold, G. (2006). Large-Eddy Simulations of Trade Wind Cumuli: Investigation of Aerosol Indirect Effects. *Journal of the Atmospheric Sciences*, *63*(6), 1605-1622. 10.1175/jas3706.1

Yang, F., Shaw, R., & Xue, H. (2016). Conditions for super-adiabatic droplet growth after entrainment mixing. *Atmospheric Chemistry and Physics*, *16*(14), 9421-9433. 10.5194/acp-16-9421-2016

Yang, P., K.-N. Liou, L. Bi, C. Liu, B. Yi, & B. A. Baum (2015), On the radiative properties of ice clouds: Light scattering, remote sensing, and radiation parameterization, *Advances in Atmospheric Sciences*, *32*(1), 32-63.

Yeom, J. M., Yum, S. S., Liu, Y., & Lu, C. (2017). A study on the entrainment and mixing process in the continental stratocumulus clouds measured during the RACORO campaign. *Atmospheric research*, *194*, 89-99. 10.1016/j.atmosres.2017.04.028

Yin, Y., Levin, Z., Reisin, T. G., & Tzivion, S. (2000). The effects of giant cloud condensation nuclei on the development of precipitation in convective clouds — a numerical study. *Atmospheric research*, *53*(1–3), 91-116.

Yum, S. S. (1998). Cloud droplet spectral broadening in warm clouds: An observational and model study. *Thesis University of Nevada*, 4878.

Yum, S. S., & Hudson, J. G. (2001). Microphysical relationships in warm clouds. *Atmospheric research*, *57*(2), 81-104.

Yum, S. S., & Hudson, J. G. (2005). Adiabatic predictions and observations of cloud droplet spectral broadness. *Atmospheric research*, *73*(3-4), 203-223. doi:10.1016/j.atmosres.2004.10.006

Yum, S. S., Wang, J., Liu, Y., Senum, G., Springston, S., McGraw, R., & Yeom, J. M. (2015). Cloud microphysical relationships and their implication on entrainment and mixing mechanism for the stratocumulus clouds measured during the VOCALS project. *Journal of Geophysical Research: Atmospheres*, *120*(10), 5047-5069. 10.1002/2014JD022802

Zhang, F., Wu, K., Li, J., Zhang, H., & Hu, S. (2018a). Radiative transfer in the region with solar and infrared spectra overlap. *Journal of Quantitative Spectroscopy and Radiative Transfer*, *219*, 366-378.

Zhang, F., Yan, J.-R., Li, J., Wu, K., Iwabuchi, H., & Shi, Y.-N. (2018b). A new radiative transfer method for solar radiation in a vertically internally inhomogeneous medium. *Journal of the Atmospheric Sciences*, *75*(1), 41-55.

Zhang, G. J., Song, X., & Wang, Y. (2019). The double ITCZ syndrome in GCMs: A coupled feedback problem among convection, clouds, atmospheric and ocean circulations. *Atmospheric research: Atmospheres*, *229*, 255-268. 10.1016/j.atmosres.2019.06.023

Zhang, M., Bretherton, C. S., Blossey, P. N., Austin, P. H., Bacmeister, J. T., Bony, S., et al. (2013). CGILS: Results from the first phase of an international project to understand the physical mechanisms of low cloud feedbacks in single column models. *Journal of Advances in Modeling Earth Systems*, *5*(4), 826-842. 10.1002/2013ms000246

Zhao, C., Tie, X., Brasseur, G., Noone, K. J., Nakajima, T., Zhang, Q., et al. (2006). Aircraft measurements of cloud droplet spectral dispersion and implications for indirect aerosol radiative forcing. *Geophysical Research Letters*, *33*(16), L16809. 10.1029/2006gl026653

Zhao, C., Zhao, L., & Dong, X. (2019). A case study of stratus cloud properties using in situ aircraft observations over Huanghua, China. *Atmosphere*, *10*(1), 19.

Table 1. Parameters of initial cloud droplet size distributions (CDSDs).

Initial CDSD	Shape of CDSD, μ	Liquid water content, LWC (g m^{-3})	Volume-mean radius, r_v (μm)	Number concentration, n_d (cm^{-3})	Relative dispersion of CDSD, d
Monodisperse	-	0.5	10.0	119.4	0.0
Narrow polydisperse	40.0	0.5	10.0	119.4	0.16
	10.0				0.30
Broad polydisperse	2.0	0.5	10.0	119.4	0.55
	0.5				0.70

Table 2. Parameters of the Explicit Mixing Parcel Model (EMPM) setting.

Parameters	Values
Domain size, D	20 m
Entrained blob size, l	2 m
Vertical velocity, w	0 m s^{-1}
Entrained air relative humidity, RH_e	60.5%, 66.0%, 71.5%, 77.0%, 82.5% (control), 88.0%
Dissipation rate, ε	1×10^{-5}, 5×10^{-3} (control), 1×10^{-2} m^2s^{-3}
Entrained air fraction, f	0.1, 0.2 (control), 0.3
Total case number	216
Case number satisfying cloud criteria	143 (66.2%)

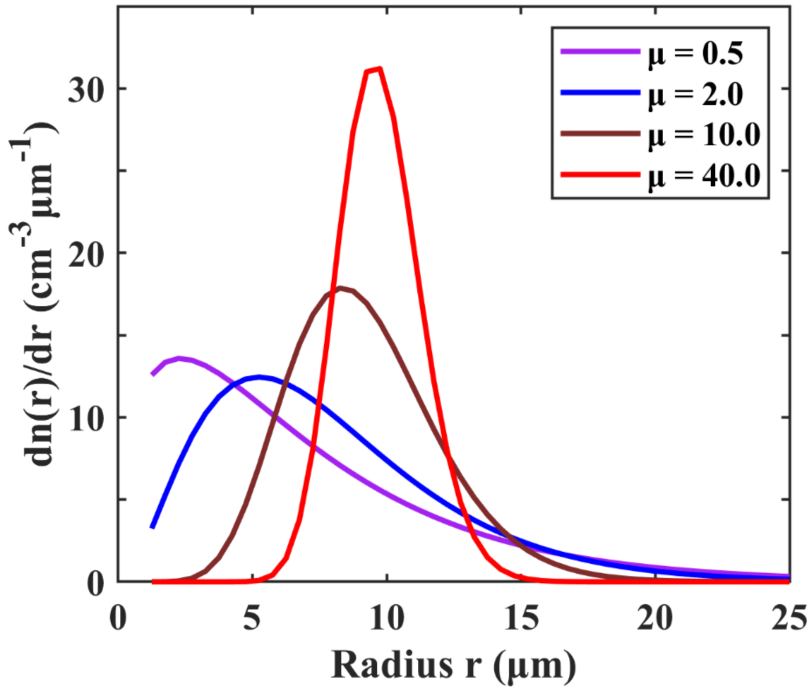

Figure 1. The initial CDSDs for different shape parameters (μ) in Table 1, with droplet number concentration of 119.4 cm^{-3}, volume-mean radius of 10.0 μm and liquid water content of 0.5 g m^{-3}.

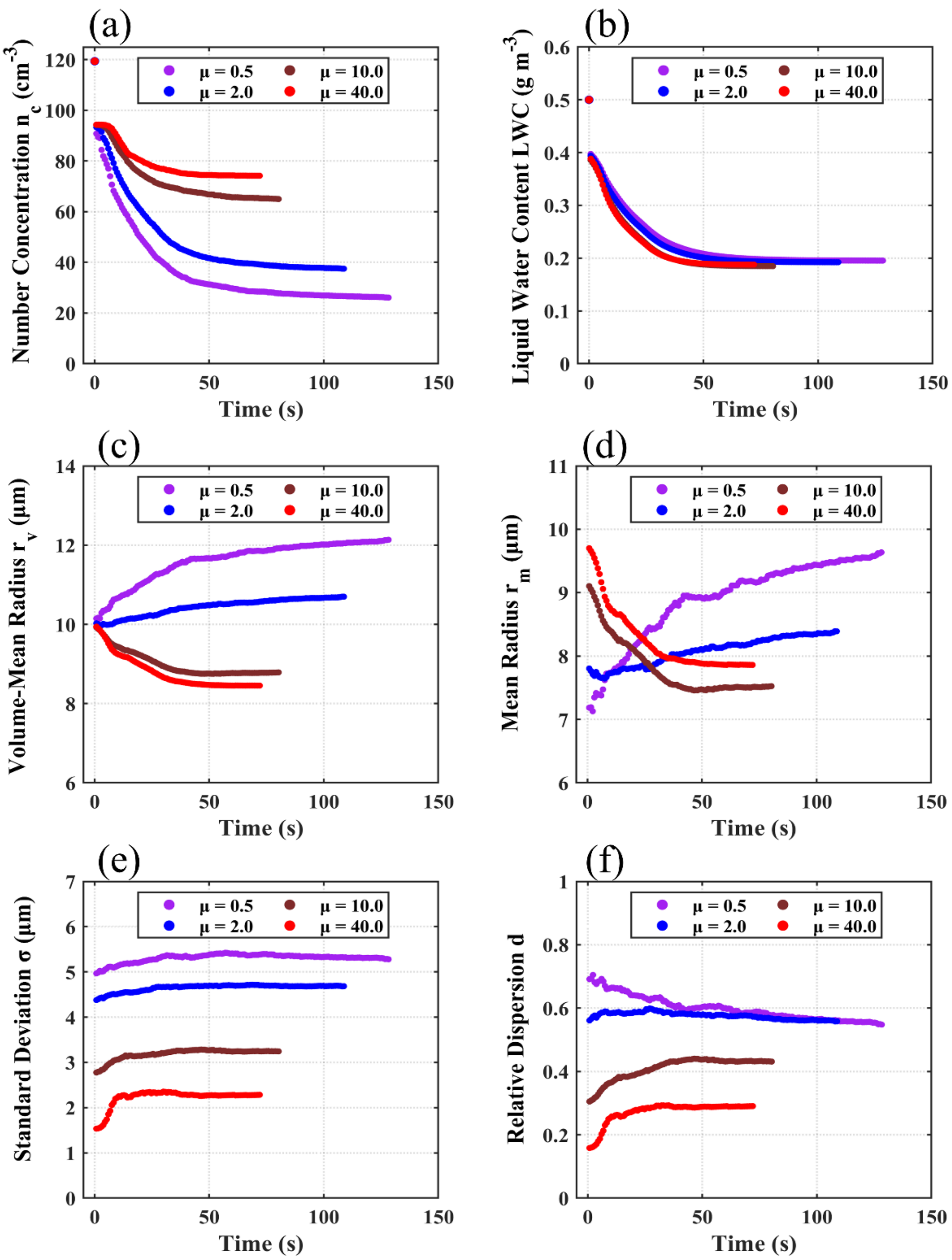

Figure 2. Temporal evolutions of (a) number concentration (n_c), (b) liquid water content (LWC), (c) volume-mean radius (r_v), (d) mean radius (r_m), (e) standard deviation (σ), and (f) relative dispersion (d) for different cloud droplet size distribution shape parameters (μ). The model input parameters are shown in the control run of Table 2.

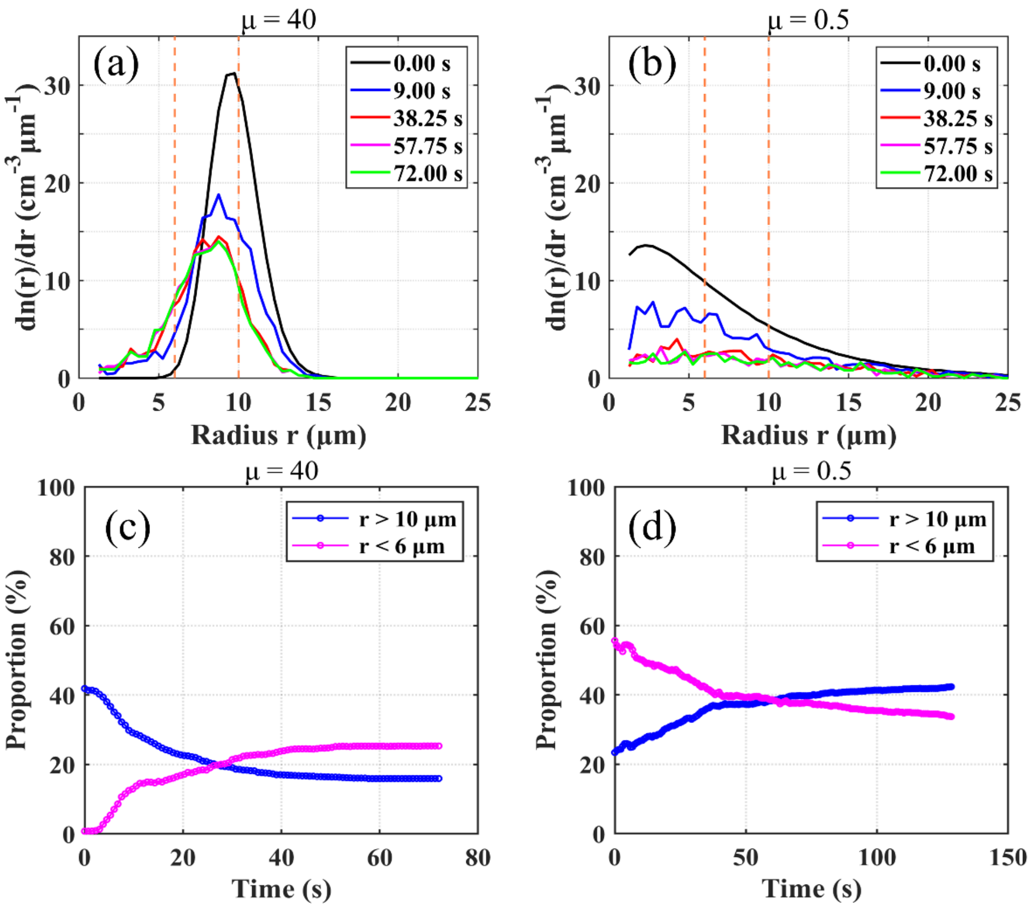

Figure 3. (a) and (b) Temporal evolution of CDSDs with their shape parameters (μ) equal to 40.0 and 0.5, respectively. (c) and (d) Temporal evolution of the ratios of big and small droplet number concentrations to the total droplet number concentration, respectively. The criteria for big and small droplets are radius (r) larger than 10 μm and smaller than 6 μm, respectively, which are shown as the vertical dash lines. The model input parameters are shown in the control run of Table 2.

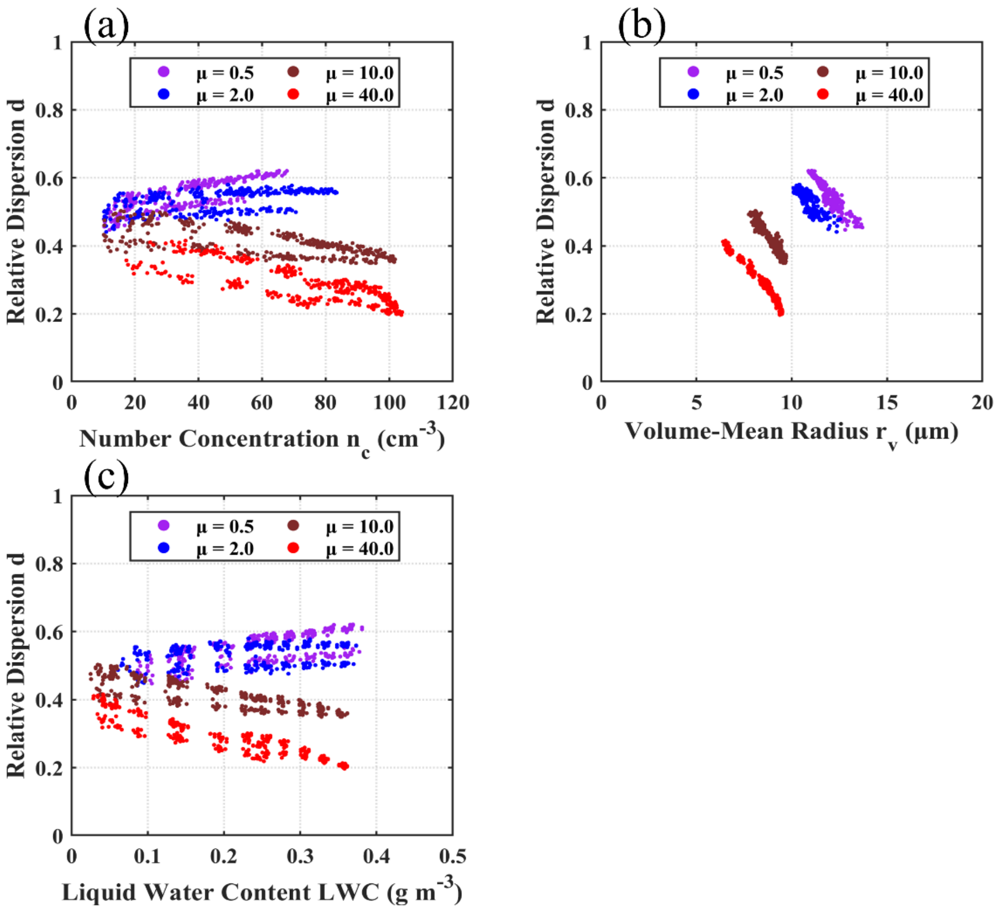

Figure 4. Relationships between relative dispersion (d) and number concentration (n_c), volume-mean radius (r_v), and liquid water content (LWC) for different cloud droplet size distribution shape parameters (μ) as listed in Table 2.

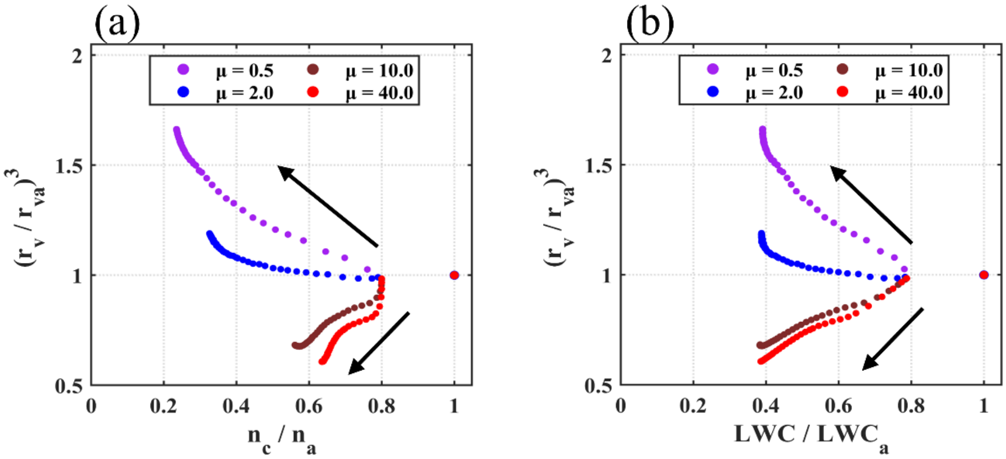

Figure 5. (a) Relationship between r_v^3/r_{va}^3 and n_c/n_a, and (b) relationship between r_v^3/r_{va}^3 and LWC/LWC$_a$ for different cloud droplet size distribution shape parameters (μ). The time direction is represented by the four arrows. The model input parameters are shown in the control run of Table 2.

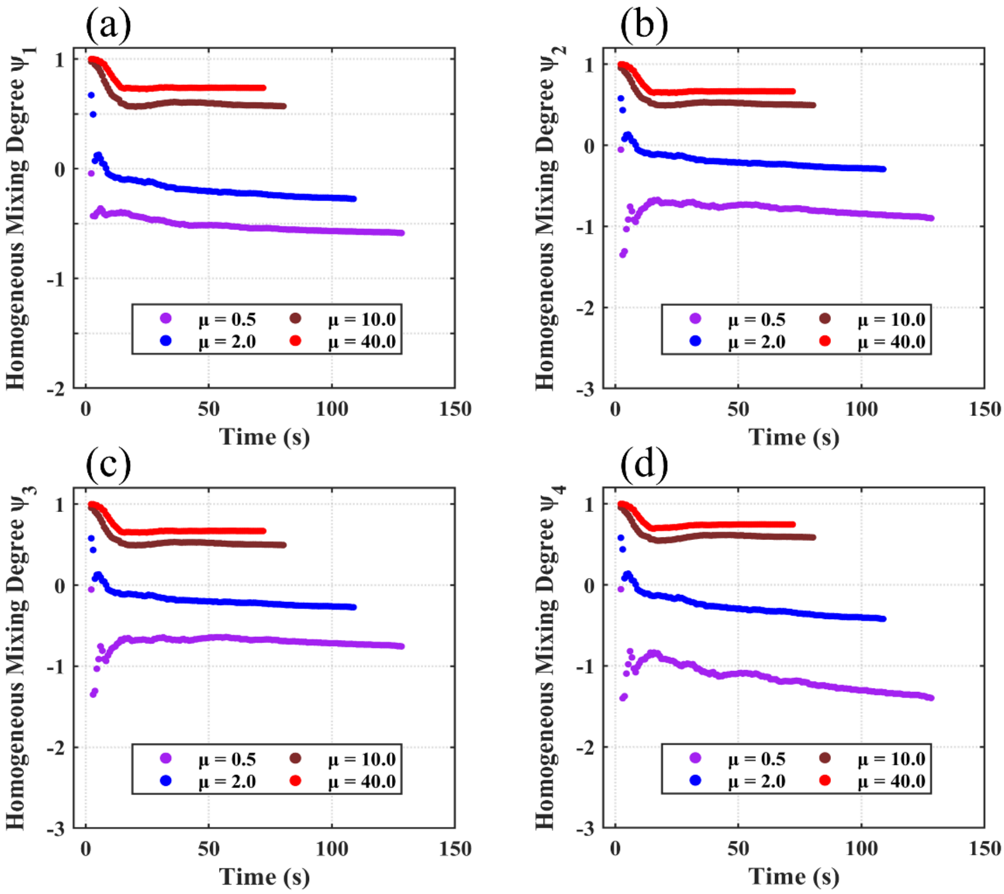

Figure 6. Temporal evolutions of traditional homogeneous mixing degrees (ψ_1, ψ_2, ψ_3, ψ_4) for different cloud droplet size distribution shape parameters (μ). The model input parameters are shown in the control run of Table 2.

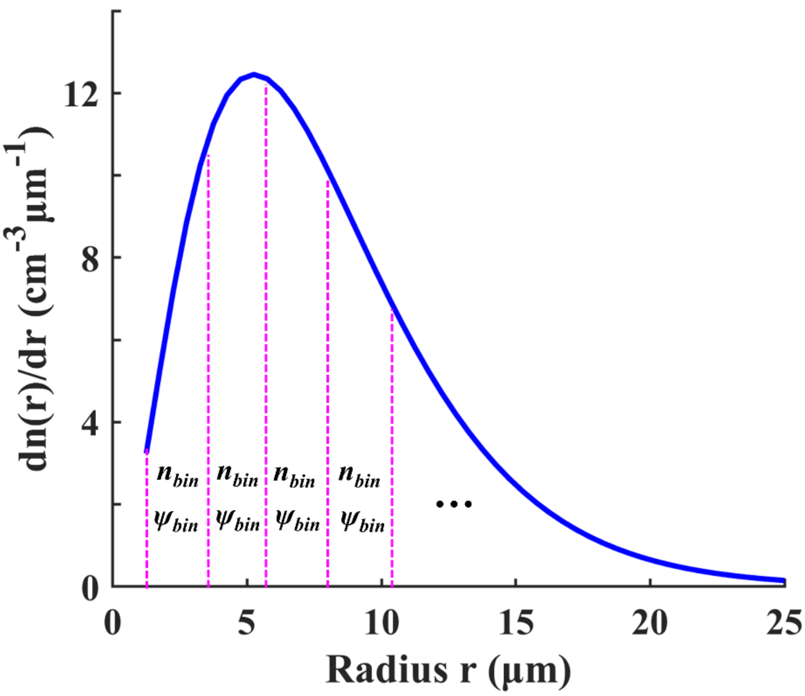

Figure 7. Schematic for defining the bin-weighted homogeneous mixing degree. The blue CDSD represents an instantaneous CDSD during entrainment-mixing for every time step. Number concentration (n_{bin}) and homogeneous mixing degree (ψ_{bin}) of the droplets in each radius bin are used to calculate the bin-weighted homogeneous mixing degree. The radius bins are divided according to the initial CDSD. See text for the detailed explanation.

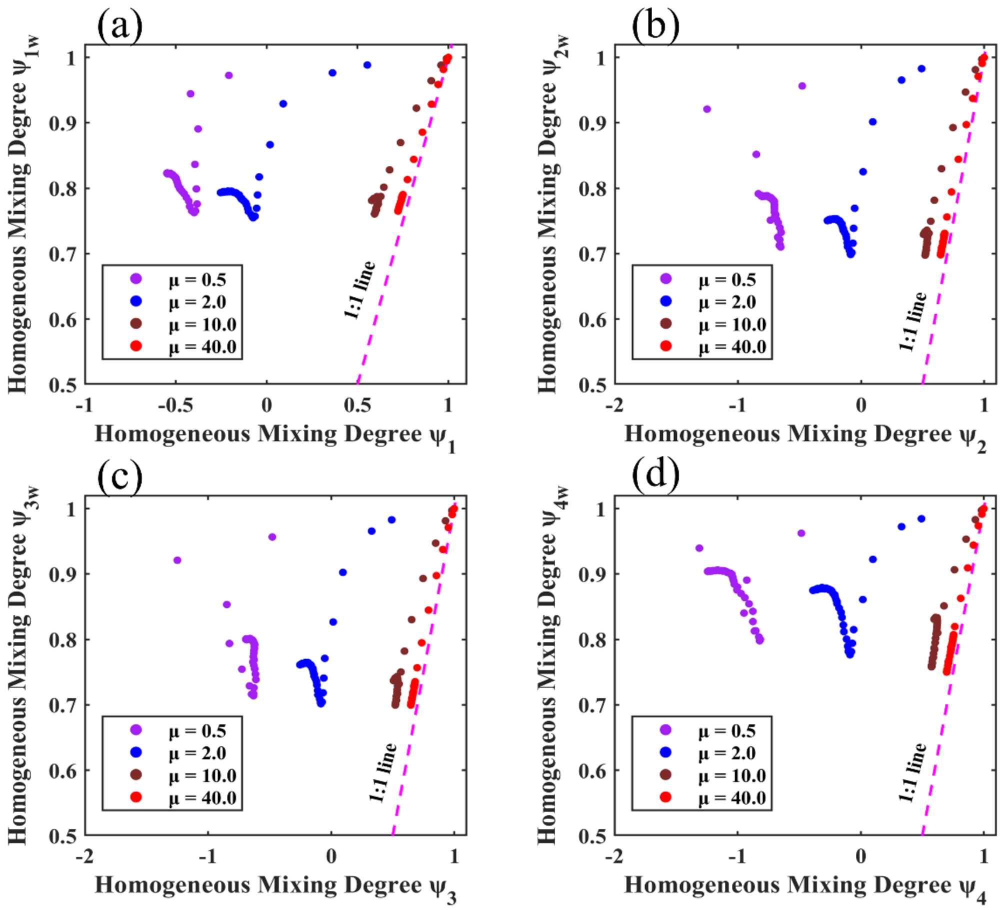

Figure 8. Relationships between bin-weighted homogeneous mixing degrees ($\psi 1_w$, $\psi 2_w$, $\psi 3_w$, $\psi 4_w$) and traditional homogeneous mixing degrees ($\psi 1$, $\psi 2$, $\psi 3$, $\psi 4$) for different cloud droplet size distributions with the shape parameters (μ) equal to 0.5, 2.0, 10.0, and 40.0. The model input parameters are shown in the control run of Table 2.

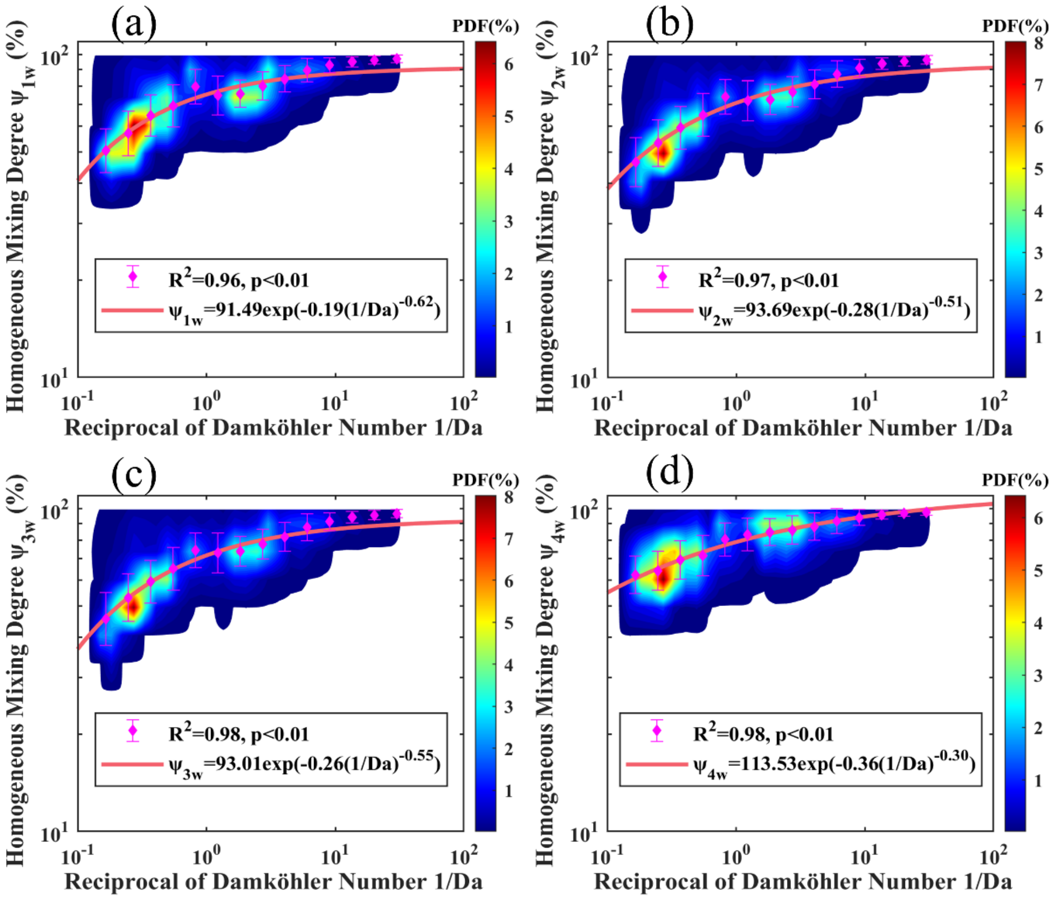

Figure 9. Joint probability density functions (PDFs) of the relationships between bin-weighted homogeneous mixing degrees and the reciprocal of Damköhler number (1/Da) of all simulated cases in Table 2. The mean values of bin-weighted homogeneous mixing degrees (diamond data points) are fitted with R^2 and p-value representing the determination coefficient and significance level, respectively. The standard deviations of bin-weighted homogeneous mixing degrees are shown as the error bars.

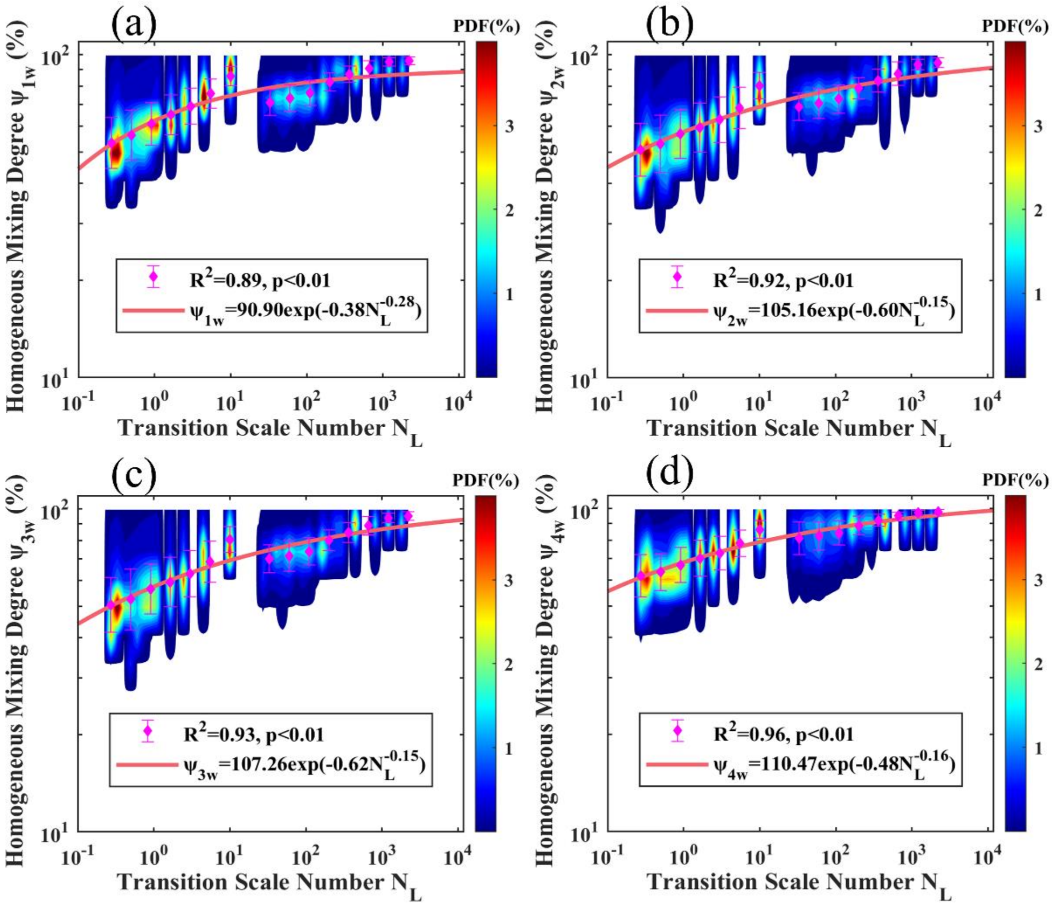

Figure 10. Same as Figure 9 but for N_L.

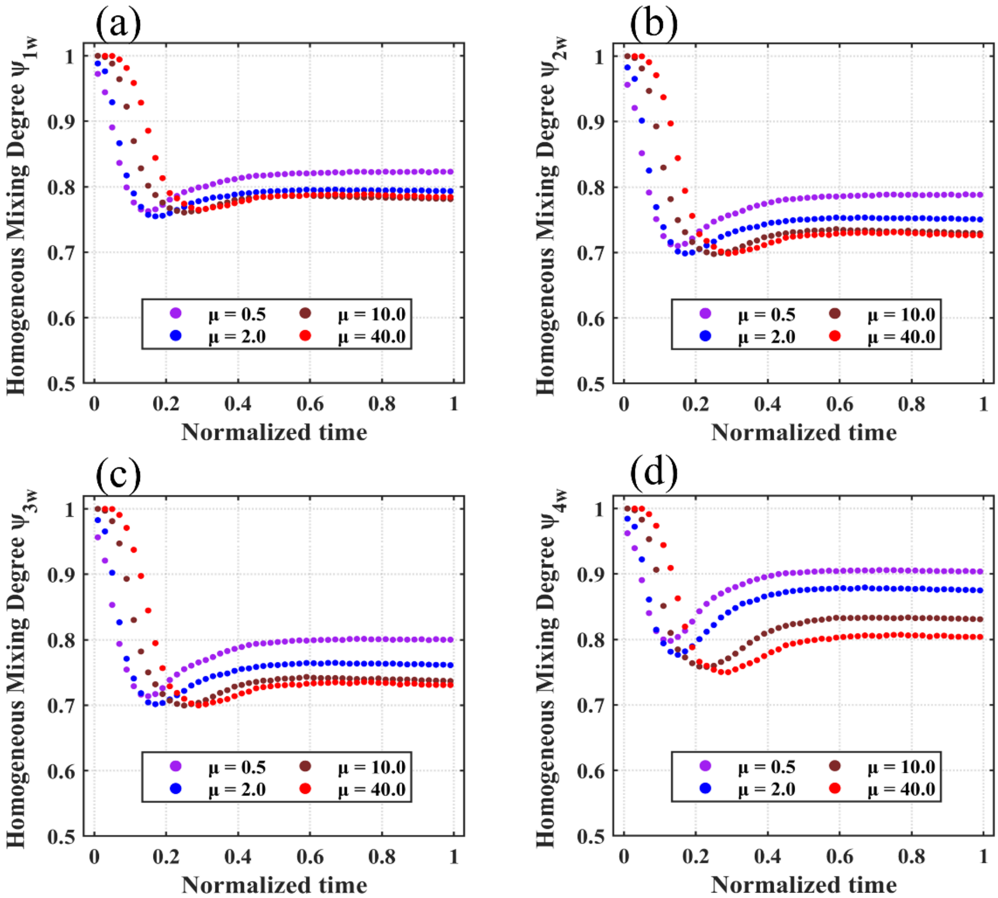

Figure 11. Temporal evolutions of bin-weighted homogeneous mixing degrees for different cloud droplet size distribution shape parameters (μ). The model input parameters are shown in the control run of Table 2.